Turkish Journal of Earth Sciences (Turkish J. Earth Sci.), Vol. 18, 2009, pp. 583–613. Copyright ©TÜBİTAK
doi:10.3906/yer-0711-2 First published online 17 August 2009

Subduction-related Eocene Shoshonites from the Cenozoic Urumieh-Dokhtar Magmatic Arc (Qaleh-Khargooshi Area, Western Yazd Province, Iran)

GHODRAT TORABI

Department of Geology, University of Isfahan, Isfahan, Iran

(E-mail: Torabighodrat@yahoo.com)

Received 07 March 2008; revised typescript received 03 July 2009; accepted 04 July 2009

Abstract: The fifth phase of Eocene volcanism in the central part of the Urumieh-Dokhtar magmatic arc (UDMA), comprises lavas with shoshonitic characteristics, ranging from trachybasalt to trachydacite. In shoshonites of the Qaleh-Khargooshi area, leucite changes to analcime, analcime to albite, sanidine to albite and anorthoclase, and clinopyroxene to albite. These reactions, together with other field, petrographic and geochemical features, are evidence of an original absarokitic magma which was changing to generate the different rock units. The parental magma of these shoshonites was produced by a low degree of partial melting from a metasomatized enriched mantle source. During the ascent of shoshonitic magma through the continental crust, crustal contamination, chemical changes and mineralogical transformations took place. The geochemistry of these shoshonitic rocks is similar to potassic volcanic rocks of continental arcs or convergent margins.

Key Words: shoshonite, Eocene, Urumieh-Dokhtar, Qaleh-Khargooshi, Iran

Senozoyik Urumieh-Dokhtar Magmatik Yayı'ndan Dalma-batma İlişkili Eosen Şoşonitleri (Qaleh-Khargooshi Bölgesi, Batı Yazd Eyaleti, İran)

Özet: Urumieh-Dokhtar magmatik yayının (UDMA) orta kesimlerindeki Eosen volkanizmasının beşinci evresi trakibazaltan trakidasite kadar değişen şoşonitik karakterli lavları içermektedir. Qaleh-Khargooshi bölgesinin şoşonitlerinde lösit analsime, analsim albite, sanidin albit ve anortoklasa ve klinopiroksen de albite değişir. Bu reaksiyonlar ile arazi, petrogragik ve jeokimyasal özellikler birlikte farklı kaya birimlerini oluşturmak üzere değişime uğrayan orijinal absarokitik magmanın verilerini oluşturmaktadır. Bu şoşonitlerin kaynak magması metasomatize zenginleşmiş manto kaynağının düşük dereceli kısmi ergimeye uğraması sonucu oluşmuştur. Kıta kabuğu boyunca yükselen şoşonitik magmada kabuk kirlenmesi, kimyasal değişimler ve mineral dönüşümleri de gerçekleşmiştir. Şoşonitik kayaçların jeokimyası kıtasal yay veya çarpışan kıta kenarlarındaki potasik volkanik kayaçlarla benzerlik sunmaktadır.

Anahtar Sözcükler: şoşonit, Eosen, Urumieh-Dokhtar, Qaleh-Khargooshi, İran

Introduction

The Qaleh-Khargooshi area belongs structurally to the central Iran zone, comprising a patchwork of horsts and grabens, between the folded zones of Zagros to the southwest and of Kopeh Dagh to the northeast. Block-faulting tectonics has been accompanied there by numerous and voluminous volcanic eruptions, particularly during the Eocene, but also during Neogene and Quaternary times. The volcanic range thus generated, called the Urumieh-Dokhtar magmatic arc (UDMA) trends NW–SE and forms the southwestern fringe of the Central Iran Zone; it extends for almost 2000 km and is continued to the northwest by the Little Caucasus and the Anatolian mountain ranges.

The area studied is situated in the central part of the Cenozoic UDMA (Figure 1). The Moho depth beneath the Qaleh-Khrgooshi area is about 42 km

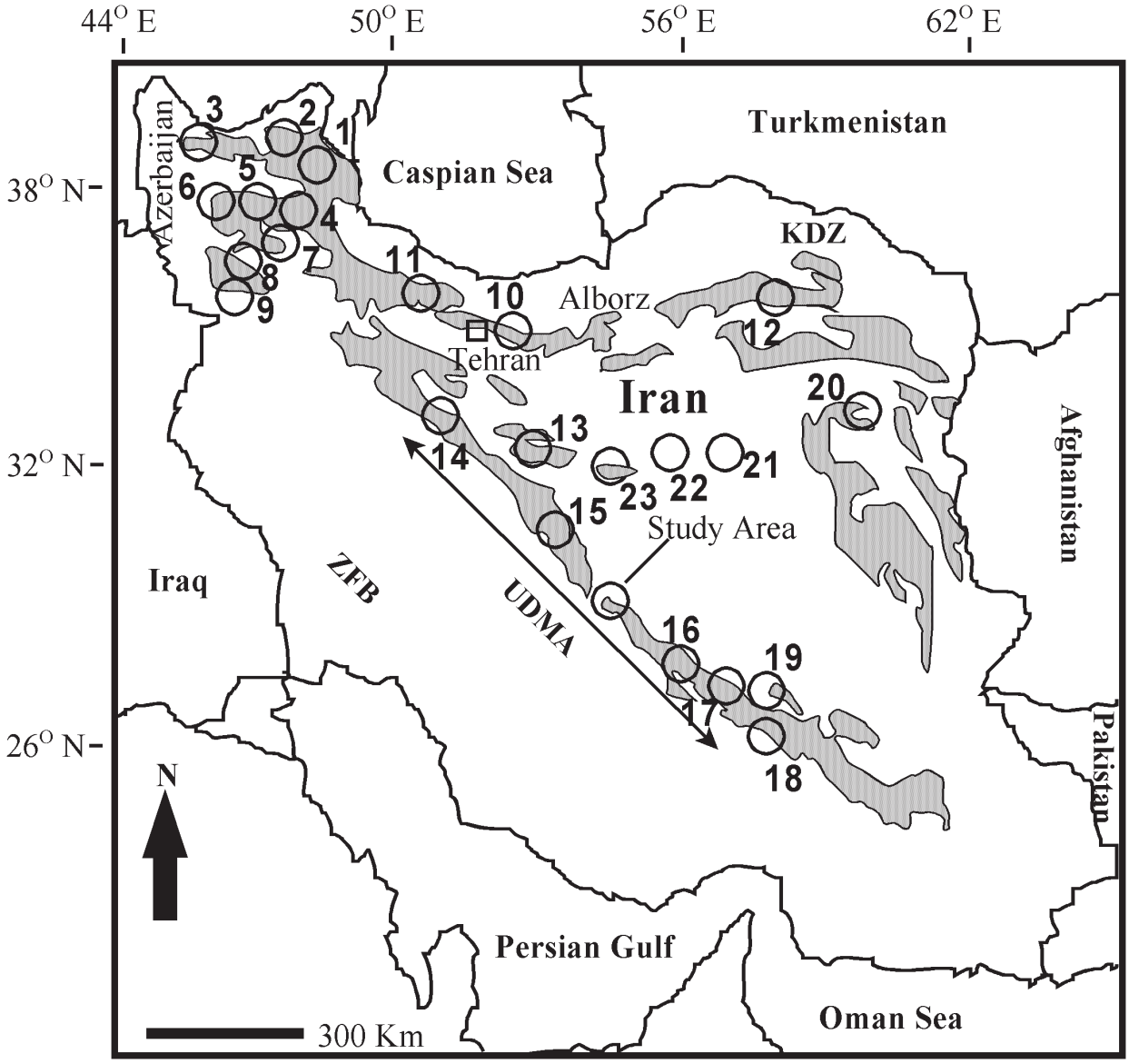

Figure 1. The main exposures of shoshonites in Iran. Numbers are related to Table 1. ZFB– Zagros folded belt; KDZ– Kopeh Dagh zone; UDMA– Urumieh-Dokhtar magmatic belt.

(Dehghani & Markis 1983). Geochemically, the volcanic rocks of Urumieh-Dokhtar are very similar to those of subduction- or continental arc-related rocks. This magmatic belt is interpreted as a continental volcanic arc formed above the northward subduction of Neothethys oceanic crust (Alavi 1994).

The Eocene volcanic rocks of the area studied, are basic to acid in composition. Effusive volcanic activity is less common, but explosive volcanism appears to have played a major role. The simultaneous presence of submarine and subaerial volcanics in both time and space, is an indication of a very active environment. Thick, rapidly accumulated sediments, volcano-sedimentary rocks, pyroclastics and lava flows were deposited in subsiding basins. The Eocene formations are separated from the underlying older rocks by a marked erosional angular unconformity (Amidi *et al.* 1984).

There are very good exposures of shoshonitic rocks in Iran (Mehdizadeh *et al.* 2002). The shoshonitic volcanic associations in Iran are limited to volcanic belts of Eocene to Recent volcanism, and are exposed in Azerbaijan province (i.e. Mianeh, Saray, Sahand, Sabalan, Takab-Qorveh), the Alborz area (Taleghan-Alemot, Damavand), the Urumieh Dokhtar zone (Qom-Aran, Saveh, Natanz-Nain, Shahrebabak, Bardsir) and the eastern zone (Aftabi & Atapour 2000). The main exposures of Iranian shoshonitic rocks are presented in Figure 1 & Table 1.

The Qaleh-Khargooshi shoshonitic association formed during an extensive period of Eocene magmatic activity and contains all shoshonite group members from basic to acidic. The position of study area on the geological map is shown in Figures 2 & 3. It is situated in western Yazd province (Iran) and Qaleh-Khargooshi is the name of an abandoned old castle to the northeast of Gavkhooni lagoon.

During the Eocene, six different phases of volcanic activity occurred in the central part of the Urumieh-Dokhtar magmatic arc (Amidi 1977), comprising, in sequence, rhyolite, lower andesite,

Table 1. Location of the major shoshonitic series in Iran (numbers are plotted on Figure 1) (After Aftabi & Atapour 2000, with changes).

No.	Location	Rocks	Age	Number of eruptions
		Azerbaijan – Alborz – Sabzevar Zone (Northern Iran)		
1	NE of Azerbaijan	phonolite-shoshonite	Eocene–Oligocene	2
2	East of Azerbaijan	shoshonite-latite-tephrite	Eocene–Oligocene	1
3	Saray	basanite-leucite tephrite-analcime basanite	Late Miocene	2
4	Mianeh	analcime trachyandesite	Eocene	1
5	Bozgush	mugearite-feldspatoidal lavas	Middle Eocene	1
6	Sahand	shoshonite	Late Miocene	1
7	Sabalan	analcime trachyte	Early Eocene	1
8	Takab-Qorveh	shoshonite	Miocene	1
9	Bijar	shoshonite-latite	Oligo–Miocene	1
10	Damavand	shoshonite	Quaternary	1
11	Taleghan	analcime basanite	Eocene–Oligocene	1
12	Sabzevar	shoshonite	Miocene–Pliocene	1
		Central Iran volcanic belt		
13	Qom – Aran	shoshonite	Early – Late Eocene	2
14	Saveh	shoshonite	Eocene	–
15	South of Ardestan	absarokite – shoshonite	Eocene	1
16	Shahrebabak (Javazm)	phonolite – shoshonite – tephrite - basanite	Eocene	5
17	Shahrebabak (Mozahem)	nepheline phonolite - trachyandesite	Oligocene	1
18	Rafsanjan – Kuh-e-Rig	trachybasalt – andesite – shoshonite	Eocene	–
19	Bardsir	absarokite – shoshonite	Eocene	1
		Eastern Iran (Lut Block)		
20	north of Lut block	shoshonite	Eocene	1
21	NE of Khur	shoshonite	Late Eocene	–
22	Arusan	shoshonite	Eocene	1
23	Anarak	shoshonite	Eocene	1

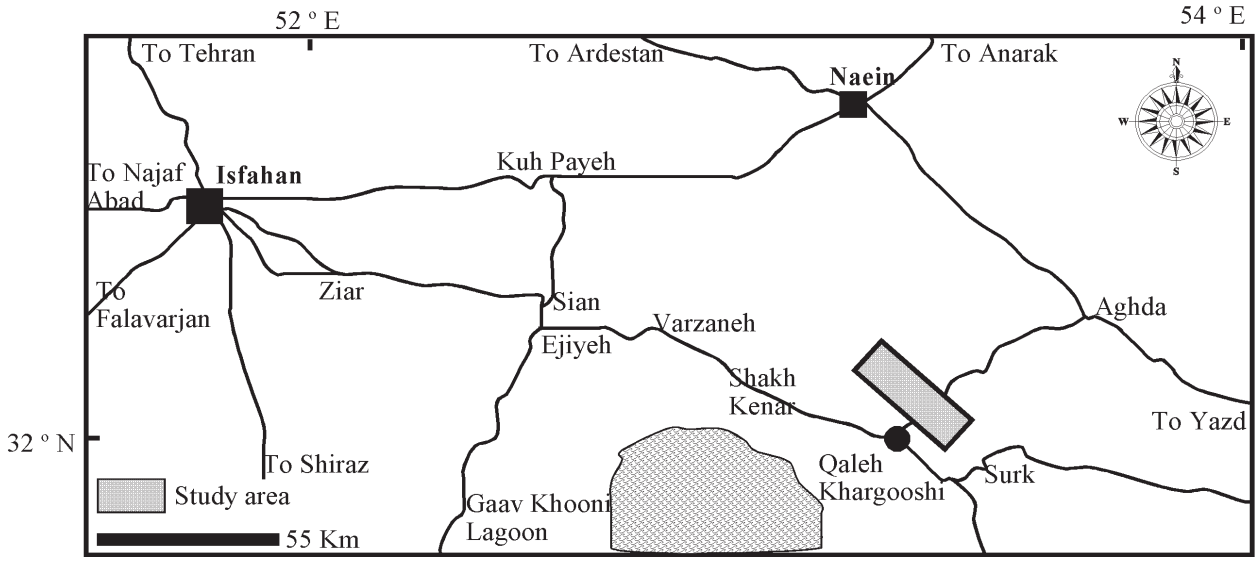

Figure 2. Roads map showing access to the study area.

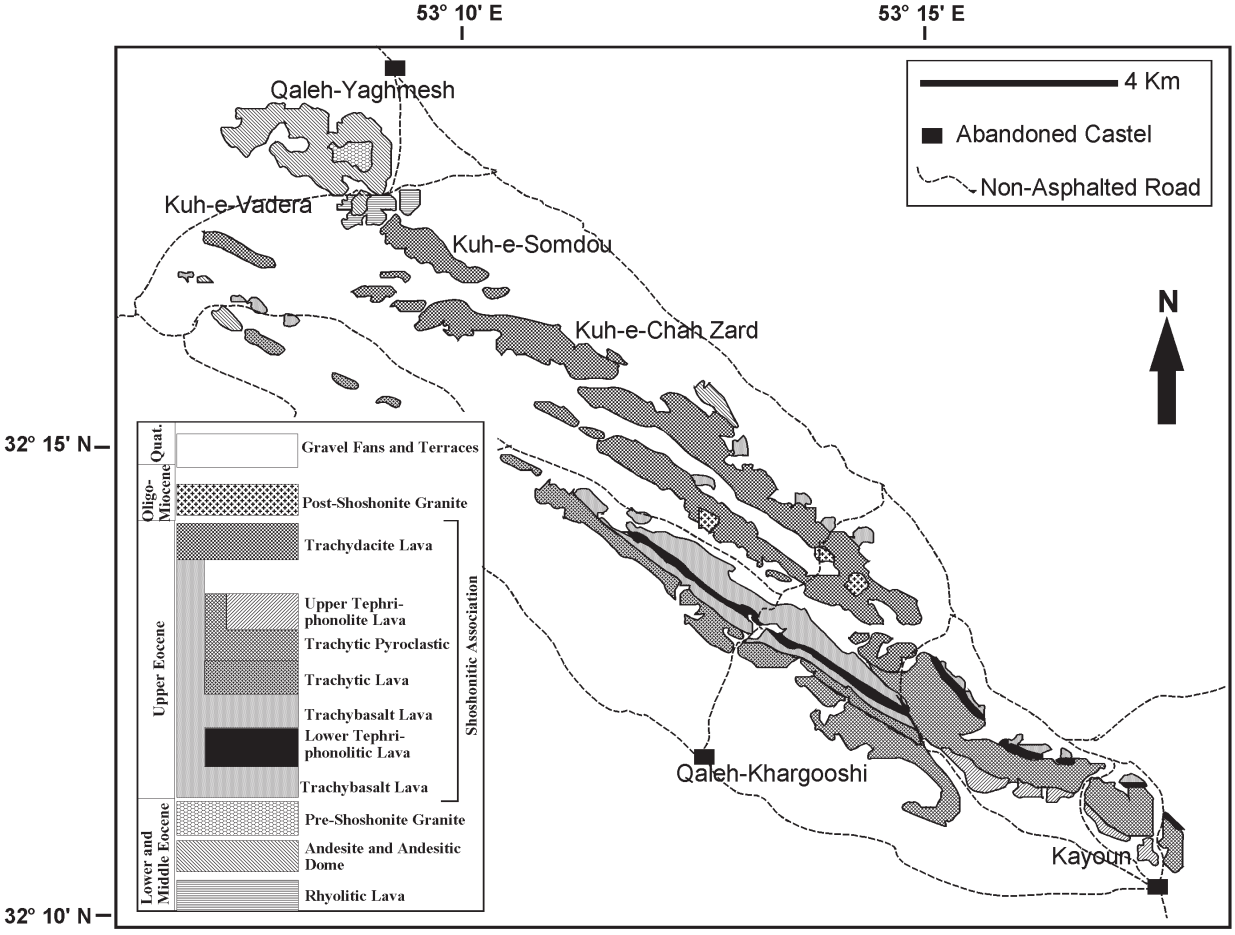

Figure 3. Geological map and stratigraphic column of the Qaleh-Khargooshi area.

rhyodacite, middle andesite, shoshonite and upper andesite (Table 2). Shoshonites of the fifth volcanic phase are Upper Eocene in age (Amidi 1977). The other volcanic activities have a calc-alkaline signature. In the Qaleh-Khargooshi area the third, fourth and fifth volcanic phases are present.

The studied area is one of the most complete exposures of shoshonitic rocks of Iran. Field photos of the studied shoshonites are shown in Figure 4. Fieldwork relationships indicate that this shoshonitic volcanism occurred in sub-aerial environment with strombolian to sub-plinian eruption type. It both postdates, and is itself intruded by granites.

This article presents a petrologic and geochemical study of the Qaleh-Khargooshi shoshonites, and discusses the mineralogical and geochemical evidences of crustal contamination and the geotectonic setting of these lavas.

Petrography

There is at present no universally adopted nomenclature for the classification of the shoshonitic suite. Iddings (1895) and Joplin (1965) used the original absarokite - shoshonite - banakite - toscanite terminology for classification, but most recent authors have resorted to an alternative scheme based on the covariation of K_2O–SiO_2 (McKenzie & Chappell 1972; Peccerillo & Taylor 1976). However, in the classification of these volcanic rocks both the mineralogical scheme of Iddings (1895) and the geochemical classification of McKenzie & Chappell (1972) and IUGS are considered.

In the IUGS geochemical classification, based on the alkalis–SiO_2 diagram, these rocks are trachybasalt, basaltic trachyandesite, phonotephrite, tephriphonolite, trachyandesite, phonolite, trachyte and trachydacite, but trachybasalt, tephriphonolite, trachyte and trachydacite are common. Detailed classification of the studied rocks is presented in the whole rock chemistry section.

Those rocks containing olivine, plagioclase and clinopyroxene as the dominant phenocryst phases in a two-feldspar, analcime, opaque phase, apatite and glass matrix are termed trachybasalt (absarokite). Those in which analcime, clinopyroxene, and plagioclase are the dominant phenocryst phases in a two-feldspar, clinopyroxene, opaque phase and glass matrix are termed tephriphonolite (shoshonite). Rocks that are basically formed by K-feldspar phenocrysts and matrix are named trachyte (banakite or latite), and rocks containing quartz, K-feldspar and plagioclase are termed trachydacite (toscanite). Photomicrographs of the studied shoshonitic rocks are presented in Figure 5.

Trachybasalts

The most distinctive petrographic feature of the Qaleh-Khargooshi shoshonitic rocks is the presence of K-feldspar.

The trachybasalts are porphyritic and dark green in hand specimen. Phenocrysts are fresh clinopyroxene, plagioclase, analcime, and idiomorphous chloritised olivine. The matrix consists of altered olivine, clinopyroxene, plagioclase, K-feldspar, analcime, magnetite, ilmenite and glass. Apatite is the most important accessory mineral. Plagioclases are tabular with a rime of sanidine (anti-rapakivi texture). Analcimes have many cracks filled by calcite. Analcime phenocrysts are euhedral and up to 4 centimetres across. Clinopyroxenes are fresh and texturally appear to be magmatic, not xenocrystal.

Secondary minerals of trachybasalts produced by hydrothermal alteration include calcite, chlorite, zeolite (mesolite), clinozoisite and celadonite.

Table 2. Eocene volcanic succession in Natanz-Surk area (Amidi 1977).

Eocene volcanic phases in Natanz-Surk region (Iran)	6	upper andesite = rhyolite + andesite + dacite
	5	shoshonitic association from trachybasalt to trachydacite
	4	middle andesite = andesite + rhyolite + rhyodacite
	3	rhyodacites
	2	lower andesite= andesite + K-andesite + dacite
	1	rhyolite + tuff and ignimbrite

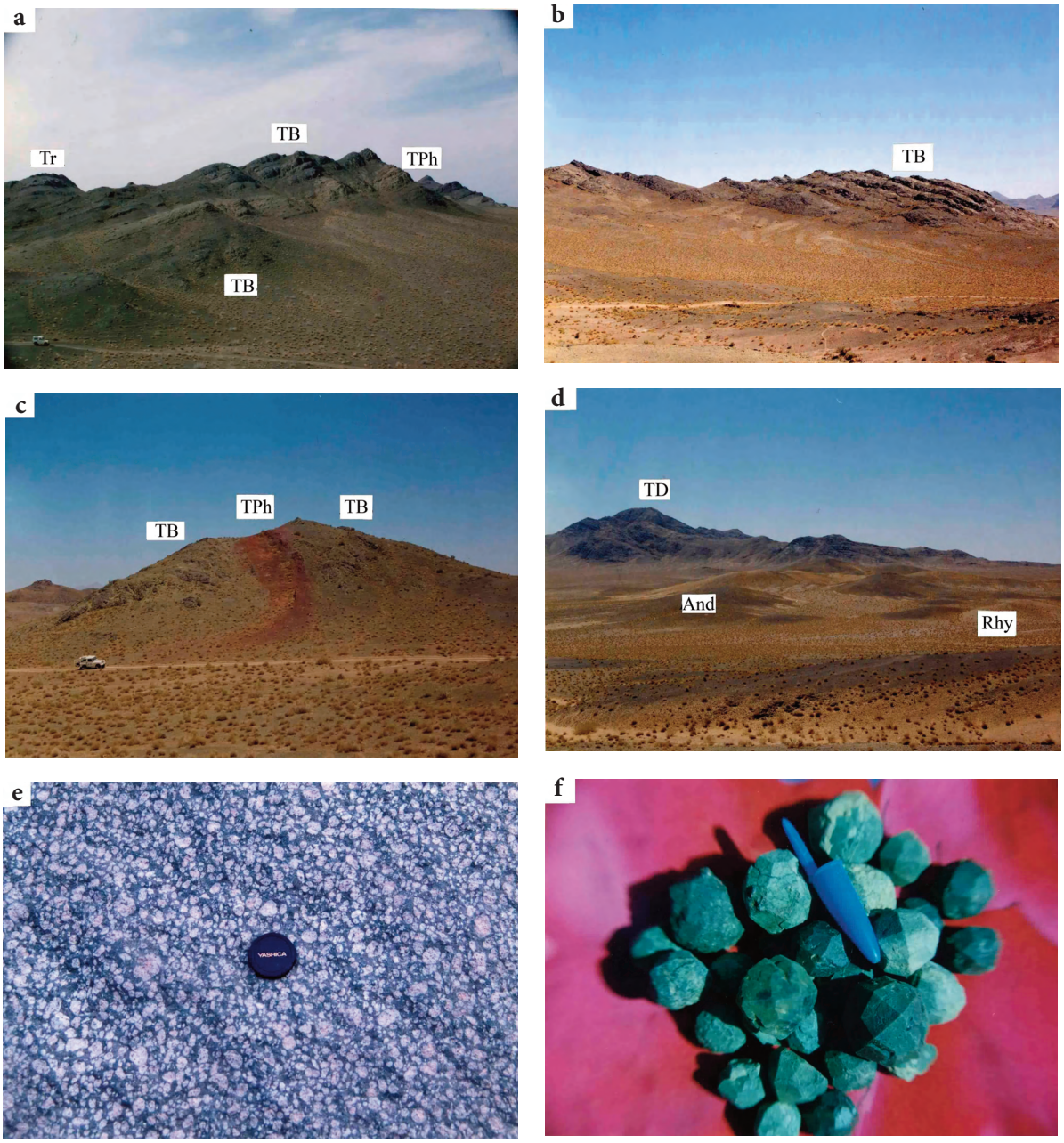

Figure 4. Field photos of the Qaleh-Khargooshi shoshonitic association. **(a–d)** Shoshonitic volcanic succession of the studied area; **(e)** abundance of analcime phenocrysts in tephriphonolite unit. 'Analcimite' term can be used for these rocks; **(f)** vecause of weathering, the analcime crystals are separated and can be gathered easily. The length of the pen lid is 6 cm. TB– trachybasalt; TPh–tephriphonolite; Tr– trachyte; TD– trachydacite; And– andesite; Rhy– rhyolite.

Tephriphonolites

Tephriphonolites are porphyritic and pale green in hand specimen. Phenocrysts are analcime and plagioclase. The matrix contains chloritized olivine, unaltered clinopyroxene, plagioclase, anorthoclase, sanidine, apatite, ilmenite, magnetite and glass. Analcime phenocrysts, up to 4 centimetres across, are euhedral. Locally, analcime is abundant and the

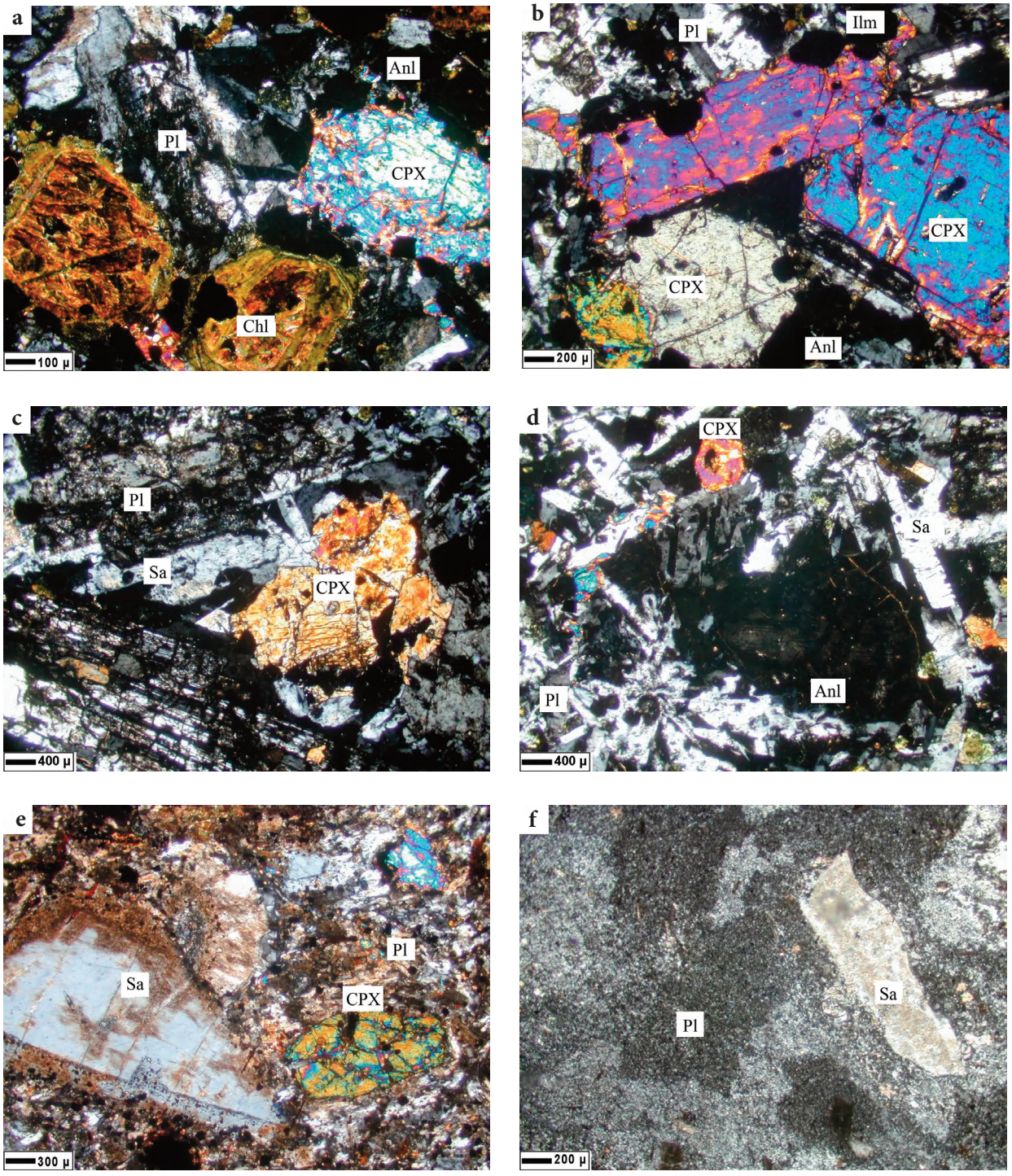

Figure 5. Microscopic photos of shoshonitic rock units. **(a, b)** Trachybasalts with clinopyroxene, chlorite, plagioclase, analcime and ilmenite; **(c, d)** clinopyroxene, plagioclase, sanidine and analcime in tephriphonolite. Plagioclases have tabular to skeletal shape; **(e, f)** trachyte containing sanidine, clinopyroxene and plagioclase. Plagioclase morphology is dendritic to spongy. Sanidines are subhedral; **(g, h)** radial plagioclase (RPl), spongy plagioclase (SPl), sanidine and quartz in trachydacite.

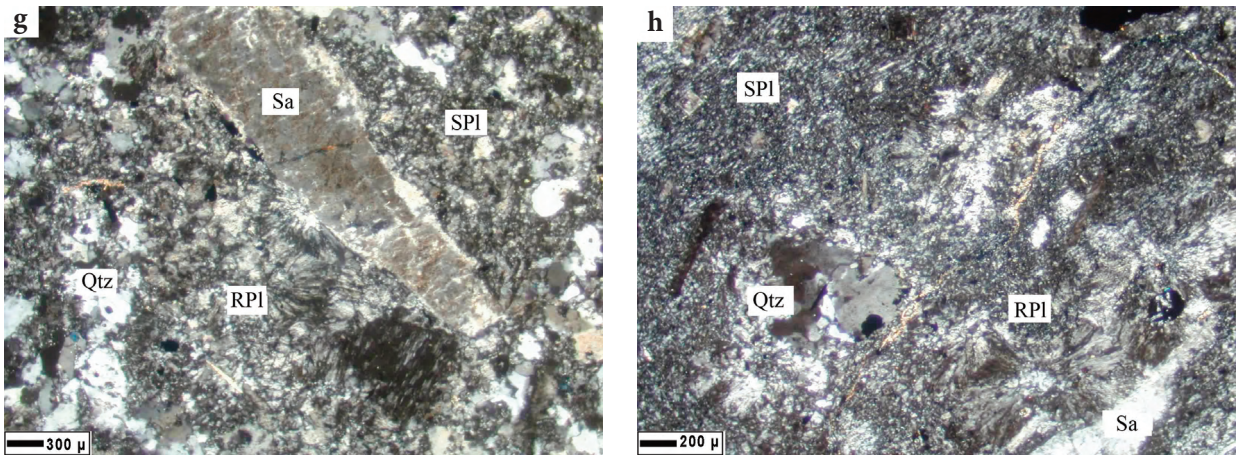

Figure 5. Continued.

term of 'analcimite' can be used. Analcimes are changed to prehnite in the contact aureoles of granite intrusions. In the central part of the area, analcime phenocrysts weather out and can be gathered easily. Some analcimes show typical leucite twinning under microscope, and all have concentric inclusions of plagioclase. Plagioclase phenocrysts are tabular to skeletal in shape and present anti-rapakivi texture. They are generally larger and more abundant than those in the trachybasalts. Most clinopyroxenes are intact.

Secondary minerals of shoshonites include prehnite, calcite, chlorite, zeolite (mesolite), datolite and muscovite.

Tephriphonolites are the best rock unit for observation of mineral exchanges. Some analcimes and clinopyroxenes are altered to albite.

Trachytes

Trachytes are pale and porphyritic, with phenocrysts of sanidine, plagioclase and clinopyroxene. Sanidine phenocrysts have a 'dusty' rim, and some are rimmed by a second growth of sanidine. With increasing SiO_2, some sanidines are altered to albite and anorthoclase. Sanidines are subhedral to anhedral and present corrosion gulf and absorption textures. The groundmass is composed of feldspar microlites. Plagioclases show dendritic to spongy morphology.

Trachydacites

The last shoshonitic eruptions in Qaleh-Khargooshi area are trachydacites. These rocks are pale and porphyritic, with sanidine and plagioclase phenocrysts. Subhedral to anhedral sanidines display corrosion gulfs or absorption textures. Plagioclases are anhedral and have spongy to radial shape. Quartz is abundant. Altered mica is present as accessory mineral. The petrography and mineralogy of these trachydacites are identical to the post-shoshonite granite that intrudes the study area.

Some mineralogical changes appear to have occurred during the ascent of shoshonitic magma through the continental crust. Petrographic evidence for these is shown in Figure 6.

Methods and Materials

Whole rock analyses were carried out in Grenoble University (France) by XRF, and at the neutron activation centre of Isfahan (Iran) by INAA. Whole rock geochemical data are presented in Tables 3 & 4. Analyses of 14 rock samples are taken from Amidi (1977) (Table 4). In analyzed whole rock samples, Mat1 is a manually separated matrix of a trachydacite, with major element composition of a trachyte.

Mineralogical analyses were conducted by wavelength-dispersive EPMA (JEOL JXA-8800R) at

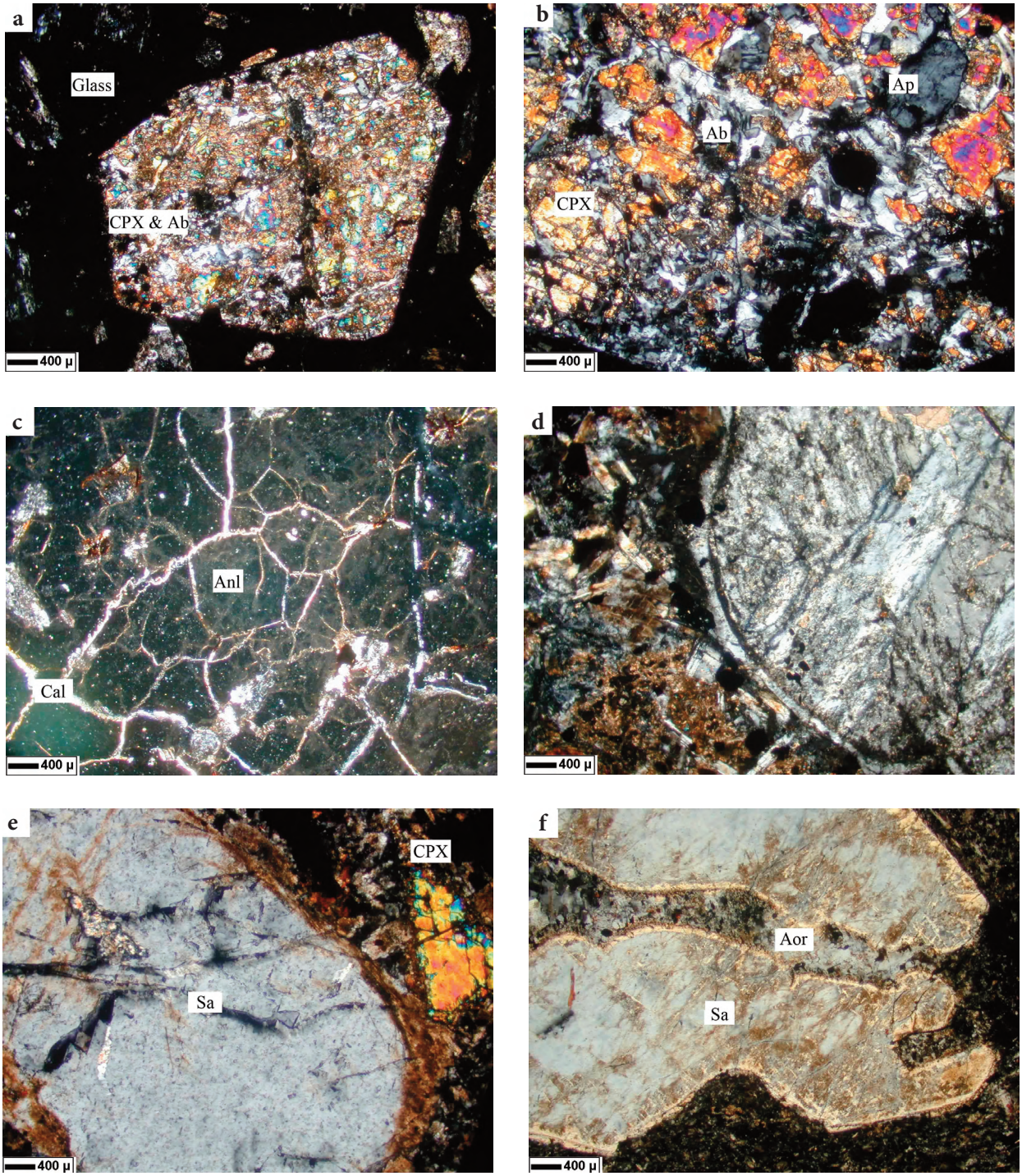

Figure 6. Mineralogical evidence for chemical exchange between the shoshonitic magma and continental crust. **(a, b)** Clinopyroxene and albite symplectite. Clinopyroxene is altered to albite with increase in SiO_2, Na_2O and Al_2O_3; **(c)** cracks in analcime crystals filled by calcite; **(d)** plagioclase phenocryst with potassic feldspar rim; **(e)** sanidine with a rim of late-generation sanidine; **(f)** sanidine in trachyte with a corrosion gulf that is partly altered to albite and anorthoclase with increase in SiO_2, Na_2O and Al_2O_3; **(g)** analcime crystal altered to albite with increasing SiO_2; **(h)** quartz, plagioclase and sanidine in trachydacite. These rocks have bands of quartz and plagioclase. Plagioclases have spongy to radial morphology. Quartz boundaries are serrated, that is the sign of disequilibrium with matrix.

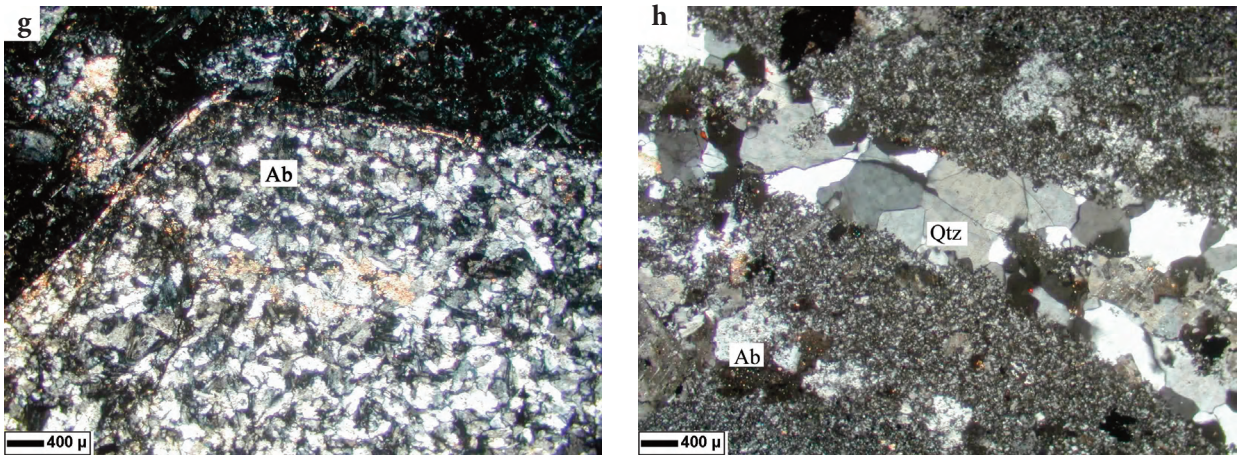

Figure 6. Continued.

the Cooperative Centre of Kanazawa University (Japan) and Leibniz University (Germany). The analyses were performed under an accelerating voltage of 15 kV and a beam current of 15 nA. The ZAF program was used for data corrections. Natural and synthetic minerals of known composition were used as standards. Representative analyses of the minerals and calculated structural formulas are shown in Table 5. Table 6 shows the results of major and trace elements of clinopyroxenes and their structural formulae.

The Fe^{3+} content in minerals was estimated by assuming mineral stoichiometry. Trace element compositions of clinopyroxenes were analyzed by a laser ablation (193 nm ArF excimer: MicroLas GeoLas Q-plus)-inductively coupled plasma mass spectrometry (Agilent 7500S) (LA-ICP-MS) at the Incubation Business Laboratory Center of Kanazawa University.

Whole Rock Chemistry

The whole rock geochemical data from Qaleh-Khargooshi shoshonites (Tables 3 & 4) show a wide range of SiO_2 contents from basic and silica-undersaturated to silica-oversaturated acidic rocks. This is confirmed by field, petrographic and mineralogical studies. Their SiO_2 contents range from 46–69 %. Their alkali contents may approach 13%. In most analyzed samples, $K_2O>Na_2O$, except in trachybasalts. The TiO_2 content of these shoshonitic rocks is low (< 0.90%). To conclude, in the area studied, the Upper Eocene volcanic rocks exhibit shoshonitic features. High LOI in the analyzed trachybasalts and tephriphonolites results from the analcime formation in these rocks.

Using different major, trace and rare earth elements, geochemical discrimination diagrams reveal that the studied rocks are alkali-enriched and belong to the shoshonitic magmatic series (Figure 7). In a total alkalis-SiO_2 diagram (Irvine & Baragar 1971) the samples plotted in the alkaline field but in the upper part, they shift to the subalkaline field (Figure 7a). The AFM diagram shows that these samples are poor in FeO* (Figure 7b). Based on a K_2O–SiO_2 diagram (McKenzie & Chappell 1972), the studied rocks are absarokite, shoshonite, banakite (latite) and toscanite (Figure 7c). In the IUGS classification (TAS diagram), the analyzed rocks are trachybasalt, basaltic trachyandesite, phonotephrite, tephriphonolite, trachyandesite, phonolite, trachyte and trachydacite (Figure 7d, Tables 3 & 4). However, most samples plot in the trachybasalt, tephriphonolite, trachyte and trachydacite fields. Therefore, in this article trachybasalt, tephriphonolite, trachyte and trachydacite, is considered equivalent to absarokite, shoshonite, banakite (latite) and toscanite, respectively. In the TAS diagram, the post-shoshonite granite lies in the rhyolite field. The Ta/Yb–Ce/Yb and Ta/Yb–Th/Yb diagrams show the shoshonitic nature of the studied samples and post shoshonite granite (Figure 7e, f).

Table 3. Whole rock chemical analyses of the Qaleh-Khargooshi shoshonites. Major elements in wt %. Trace and rare earth elements in ppm, except Au (gold) in ppb.

Sample	IUGS Name	SiO_2	TiO_2	Al_2O3	Fe_2O_3*	MnO	MgO	CaO	Na_2O	K_2O	LOI
3-10	post.sho.granite	70.04	0.50	14.18	2.87	0.07	1.08	1.40	3.92	5.57	0.50
3-8	basaltic tr.andesite	49.81	0.52	19.80	10.03	0.16	2.82	6.29	3.09	4.24	3.90
3-4	tephriphonolite	53.59	0.58	20.78	4.73	0.07	2.16	2.97	5.67	6.17	3.40
3-12	phonotephrite	52.50	0.50	15.12	5.99	0.11	2.82	9.24	2.93	6.53	4.60
3-13	tephriphonolite	54.02	0.50	14.91	6.60	0.14	1.83	7.92	3.31	6.66	4.30
3-5	phonolite	56.38	0.67	19.22	4.45	0.12	2.49	1.40	7.08	5.44	3.20
3-9	trachyte	58.50	0.52	19.01	4.59	0.11	2.51	1.97	3.65	8.11	1.00
3-1	trachyte	59.74	0.53	18.90	4.30	0.09	1.16	2.42	2.70	9.12	1.00
3-2	trachyte	62.71	0.50	17.06	3.87	0.12	1.49	1.40	3.65	7.74	1.60
4-1	trachydacite	64.46	0.50	17.92	3.22	0.07	1.49	1.40	3.55	6.29	0.30
3-11	trachydacite	66.73	0.48	15.18	2.44	0.04	0.66	1.40	4.27	8.11	0.70
3-6	trachydacite	68.33	0.50	14.36	2.87	0.05	1.33	2.10	3.10	6.40	0.60
3-7	trachydacite	68.63	0.50	14.36	2.57	0.05	1.33	1.40	3.51	6.66	0.60
Mat1	trach. dac. matrix	53.92	0.50	15.52	4.24	0.13	1.10	8.96	3.19	8.47	4.10

Sample	Cr	Co	Sc	V	Zn	Sn	W	Mo	As	Sb	Ag	Au	Rb	Cs	Ba	Sr
3-10	11	2	6	23	68	168	2.40	11.30	55.70	2.40	4.3	14.0	113	1.00	874	200
3-8	17	22	20	191	169	214	2.20	2.30	6.80	1.20	5.7	10.0	77	1.90	1500	627
3-4	17	9	4	28	96	209	2.00	4.00	4.40	1.00	4.3	35.0	270	55.60	1300	362
3-12	18	12	13	47	144	200	3.80	3.40	7.50	1.80	5.3	21.0	145	1.30	1100	267
3-13	15	13	9	56	148	184	4.20	3.80	36.60	2.00	4.6	48.0	134	1.50	1000	341
3-5	9	7	5	43	106	223	2.00	3.50	8.70	0.30	4.7	40.0	180	62.80	1300	548
3-9	7	6	5	49	88	164	2.90	7.40	6.60	0.90	3.7	34.0	250	5.90	3000	774
3-1	13	6	5	58	111	167	2.70	5.50	7.30	0.70	4.0	81.0	269	4.30	2700	152
3-2	15	4	5	24	74	166	5.80	4.70	85.30	0.73	4.0	9.0	271	6.80	791	303
4-1	10	3	8	61	97	182	4.00	6.00	40.00	0.70	4.6	37.0	247	5.40	998	200
3-11	9	1	6	23	89	150	2.00	3.50	15.60	0.77	3.6	18.0	150	1.50	653	200
3-6	13	2	6	22	85	164	2.20	2.60	54.00	1.00	3.9	40.0	188	2.20	807	150
3-7	6	2	7	24	101	148	2.00	2.30	12.40	0.75	3.6	20.0	150	3.30	722	200
Mat1	8	4	4	74	296	162	3.60	13.00	9.00	0.10	3.8	63.0	200	1.30	871	---

Table 3. Continued.

Sample	Ta	Hf	Zr	Th	U	La	Ce	Nd	Sm	Eu	Gd	Tb	Dy	Ho	Tm	Yb	Lu
3-10	1.57	7.20	126	31.50	5.30	58.32	107.12	41.02	7.00	1.20	5.35	1.03	7.30	1.62	0.71	4.40	0.67
3-8	0.90	5.00	146	28.30	4.90	44.96	76.16	33.18	6.37	1.71	3.88	0.70	4.90	0.98	0.44	2.90	0.42
3-4	0.94	4.70	136	31.00	6.40	39.16	62.56	20.38	4.00	1.10	2.97	0.38	2.20	0.50	0.22	1.51	0.23
3-12	0.61	3.90	180	13.00	8.60	25.64	43.30	15.70	4.03	1.02	3.29	0.51	2.90	0.62	0.29	1.92	0.30
3-13	0.84	4.20	180	22.60	9.00	40.09	62.58	25.37	4.73	1.30	3.38	0.54	3.00	0.59	0.28	1.70	0.26
3-5	1.10	5.50	200	30.80	7.80	37.46	59.92	23.37	3.88	1.10	2.51	0.41	3.06	0.63	0.27	2.00	0.28
3-9	1.32	7.00	150	34.80	9.00	46.12	76.60	23.80	5.50	1.50	0.00	0.79	4.28	0.82	0.36	2.30	0.36
3-1	1.40	7.30	152	32.00	10.00	44.80	77.42	27.26	5.40	1.70	4.14	0.58	3.20	0.76	0.32	2.00	0.31
3-2	2.30	10.00	303	50.20	10.00	61.76	106.92	36.30	6.70	1.20	3.97	0.65	4.24	0.98	0.43	3.02	0.45
4-1	2.10	11.00	259	45.70	10.20	69.63	115.76	43.00	8.60	1.40	5.47	1.10	7.20	1.74	0.87	5.40	0.81
3-11	1.54	7.00	200	32.00	6.30	47.82	79.71	29.87	5.43	0.90	4.10	0.85	5.48	1.33	0.59	3.60	0.54
3-6	1.80	8.70	202	32.00	6.40	52.51	88.12	32.70	5.60	1.00	4.75	0.87	6.09	1.43	0.63	3.80	0.61
3-7	1.61	7.50	111	31.60	6.20	48.30	82.29	28.61	5.03	0.88	4.08	0.86	5.53	1.35	0.60	4.00	0.60
Mat1	1.20	4.70	---	32.00	9.00	31.80	64.00	18.00	4.18	1.10	2.81	0.44	2.30	0.53	0.24	1.60	0.24

Table 4. Major and trace element chemical analyses of the Qaleh-Khargooshi shoshonites (taken from Amidi 1977).

Sample	IUGS Name	SiO_2	TiO_2	Al_2O_3	Fe_2O_3*	MnO	MgO	CaO	Na_2O	K_2O	P_2O5	H_2O	CO_2	LOI	Rb	Ba	Sr
A129	trachybasalt	46.54	0.89	17.45	10.07	0.21	6.66	9.35	3.26	2.19	0.37	2.35	0.55	0.52	50	1300	850
B130	trachybasalt	48.83	0.72	20.73	7.79	0.19	3.85	8.93	4.17	1.66	0.38	2.29	0.41	0.58	110	2000	1180
C4	trachybasalt	49.30	0.71	20.08	7.53	0.15	3.13	7.50	4.26	3.08	0.40	1.91	0.50	0.50	–	–	–
D7	trachybasalt	49.47	0.79	20.11	8.69	0.16	3.68	7.70	2.93	4.17	0.36	0.44	0.47	1.40	–	–	–
E107	phonotephrite	49.00	0.80	20.60	7.52	0.15	4.06	7.76	4.00	3.40	0.12	2.40	0.44	0.24	92	1700	1020
F131	trachybasalt	49.33	0.72	20.60	7.81	0.18	4.03	7.51	4.10	2.07	0.31	2.35	0.63	0.37	76	2000	1180
G108	tephriphonolite	52.80	0.39	19.88	4.24	0.16	2.25	4.35	4.20	7.31	0.19	3.52	0.44	0.60	282	1800	1000
H132	tephriphonolite	52.97	0.39	19.88	4.23	0.14	2.20	4.24	4.04	7.09	0.10	3.98	0.41	0.26	310	1900	1090
I110	trachyandesite	57.60	0.41	17.13	3.55	0.07	1.03	3.62	3.81	7.69	0.18	1.57	0.38	2.97	290	2000	1380
J111	trachyte	59.01	0.45	18.76	4.29	0.07	0.92	3.16	4.56	7.13	0.21	0.99	0.62	0.35	200	2000	1350
K112	phonotephrite	52.46	0.68	21.50	5.34	0.10	1.76	5.88	4.13	5.13	0.42	2.62	0.11	0.37	240	1760	1080
L144	trachyandesite	53.88	0.76	19.49	5.38	0.10	2.46	4.78	4.42	4.65	0.75	2.85	0.35	0.36	–	–	–
M2	trachydacite	65.05	0.30	17.35	2.98	0.05	0.55	2.50	4.73	5.64	0.07	0.82	0.30	0.10	–	–	–
N105	trachydacite	68.03	0.27	17.34	2.13	0.04	0.51	1.10	3.88	5.44	0.04	0.79	0.24	0.33	200	550	130

Table 5. Chemical composition (wt%) and calculated structural formulae of minerals in different shoshonitic rock units.

Rock	Trachybasalt					Tephriphonolite							
Mineral	CPX	Analcime	Plgioclase (Inner part)	Feldspar (Margin)	Sanidine	CPX	CPX	Analcime	Anorth-oclase	Albite From CPX	Albite From Analcime	Ilmenite	Apatite
SiO_2	48.28	56.91	53.93	55.40	64.94	50.19	49.47	56.38	65.21	68.04	68.25	0.14	1.08
TiO_2	0.92	0.01	0.04	0.05	0.06	0.70	1.00	0.02	0.07	0.04	0.00	18.33	0.00
Al_2O_3	5.97	22.28	28.52	22.49	19.60	3.57	5.01	22.24	19.90	20.00	19.92	2.13	0.10
Cr_2O_3	0.01	0.01	0.00	0.00	0.00	0.02	0.01	0.01	0.00	0.00	0.00	0.00	0.00
FeO*	9.43	0.13	0.59	2.31	0.20	8.89	9.46	0.13	0.30	0.03	0.02	70.86	0.35
MnO	0.24	0.00	0.00	0.05	0.00	0.33	0.25	0.01	0.00	0.00	0.00	1.08	0.07
MgO	12.26	0.00	0.04	0.40	0.00	13.34	12.55	0.00	0.01	0.00	0.00	0.00	0.28
CaO	22.27	0.72	11.42	10.55	1.46	22.08	20.89	0.51	1.31	0.60	0.51	0.13	51.27
Na_2O	0.44	11.88	4.74	1.55	4.90	0.51	0.46	12.49	8.19	11.23	11.23	0.04	0.07
K_2O	0.02	0.04	0.63	7.21	8.98	0.02	0.02	0.11	5.02	0.07	0.07	0.08	0.02
P_2O_5	0.18	0.00	0.12	0.12	0.00	0.23	0.20	0.01	0.00	0.00	0.00	0.00	37.83
NiO	0.00	0.00	0.00	0.00	0.01	0.01	0.02	0.02	0.00	0.00	0.00	0.00	0.00
Total	100.01	91.97	100.05	100.12	100.16	99.88	99.33	91.89	100.02	100.01	100.00	92.78	91.07
Oxygen	6	6	8	8	8	6	6	6	8	8	8	6	25
Si	1.80	2.13	2.44	2.61	2.93	1.87	1.86	2.10	2.90	2.98	2.99	0.01	0.19
Ti	0.03	0.00	0.00	0.00	0.00	0.02	0.03	0.00	0.00	1.00	0.00	0.72	0.00
Al	0.26	0.98	1.52	1.25	1.04	0.16	0.22	0.97	1.04	1.03	1.03	0.13	0.02
Cr	0.00	0.00	0.00	0.00	0.00	0.00	0.00	0.00	0.00	0.00	0.00	0.00	0.00
Fe^{2+}	0.18	0.00	0.02	0.09	0.01	0.18	0.26	0.00	0.01	0.00	0.00	0.65	0.05
Fe^{3+}	0.11	0.00	0.00	0.00	0.01	0.10	0.04	0.00	0.00	0.00	0.00	2.43	0.00
Mn	0.01	0.00	0.00	0.00	0.00	0.01	0.01	0.00	0.00	0.00	0.00	0.05	0.01
Mg	0.68	0.00	0.00	0.03	0.00	0.74	0.70	0.00	0.00	0.00	0.00	0.00	0.08
Ca	0.89	0.03	0.55	0.53	0.07	0.88	0.85	0.02	0.06	0.03	0.02	0.01	9.87
Na	0.03	0.86	0.42	0.14	0.43	0.04	0.03	0.90	0.70	0.95	0.95	0.00	0.02
K	0.00	0.00	0.04	0.43	0.52	0.00	0.00	0.01	0.28	0.00	0.00	0.01	0.00
P	0.00	0.00	0.01	0.01	0.00	0.00	0.00	0.00	0.00	0.00	0.00	0.00	5.75
Ni	0.00	0.00	0.00	0.00	0.00	0.00	0.00	0.00	0.00	0.00	0.00	0.00	0.00
Total	4.00	4.00	5.00	5.00	5.00	4.00	4.00	4.00	5.00	5.00	5.00	4.00	16.00

Rock	Trachyte			Trachydacite
Mineral	CPX	Sanidine (Inner)	Sanidine (Outer)	Sanidine
SiO_2	52.04	65.63	64.80	64.96
TiO_2	0.49	0.04	0.06	0.00
Al_2O_3	2.46	19.12	19.37	18.34
Cr_2O_3	0.00	0.01	0.02	0.00
FeO*	9.37	0.17	0.19	0.00
MnO	0.56	0.00	0.02	0.00
MgO	13.04	0.00	0.00	0.00
CaO	21.25	0.64	0.87	0.00
Na_2O	0.48	3.69	2.68	0.61
K_2O	0.01	10.54	11.65	16.10
P_2O_5	0.16	0.00	0.00	0.00
NiO	0.01	0.00	0.00	0.00
Total	99.84	99.85	99.66	100.02
Oxygen	6	8	8	8
Si	1.95	2.99	2.98	3.00
Ti	0.01	0.00	0.00	0.00
Al	0.11	1.03	1.05	1.00
Cr	0.00	0.00	0.00	0.00
Fe^{2+}	0.29	0.01	0.01	0.00
Fe^{3+}	0.00	0.00	0.00	0.00
Mn	0.02	0.00	0.00	0.00
Mg	0.73	0.00	0.00	0.00
Ca	0.85	0.03	0.04	0.00
Na	0.04	0.33	0.24	0.05
K	0.00	0.61	0.68	0.95
P	0.00	0.00	0.00	0.00
Ni	0.00	0.00	0.00	0.00
Total	4.00	5.00	5.00	5.00

Table 6. Chemical composition of clinopyroxenes (major elements in wt%, trace elements in ppm) in the Qaleh-Khargooshi shoshonitic rock units and their structural formula.

Sample	Rock	SiO_2	TiO_2	Al_2O_3	Cr_2O_3	FeO*	MnO	MgO	CaO	Na_2O	K_2O	NiO	Total	Mg#
8	trachybasalt	50.41	0.99	3.74	0.05	9.97	0.32	12.93	21.33	0.62	0.01	0.00	100.37	0.752
8		50.98	0.87	3.66	0.06	9.66	0.28	13.18	21.52	0.55	0.02	0.00	100.78	0.750
8		50.25	0.83	4.17	0.01	9.98	0.30	12.94	21.63	0.56	0.02	0.01	100.70	0.765
8		51.00	0.79	3.88	0.00	9.56	0.29	13.37	21.55	0.54	0.03	0.01	101.02	0.764
8		49.61	1.09	4.83	0.00	9.86	0.31	12.47	21.45	0.54	0.02	0.00	100.18	0.742
9	trachybasalt	50.49	0.90	4.36	0.02	9.95	0.30	12.79	21.33	0.54	0.01	0.01	100.70	0.735
9		50.71	0.89	4.18	0.03	9.45	0.29	13.07	21.89	0.55	0.01	0.01	101.08	0.763
9		50.02	0.95	4.61	0.00	9.48	0.28	12.85	22.01	0.46	0.04	0.01	100.71	0.765
9		50.05	1.01	4.02	0.00	9.30	0.30	12.98	21.77	0.43	0.01	0.00	99.87	0.757
11	tephriphonolite	49.05	1.06	5.90	0.01	9.34	0.28	12.70	21.58	0.56	0.01	0.02	100.51	0.780
11		49.29	1.07	5.67	0.01	9.48	0.28	12.66	21.41	0.65	0.02	0.01	100.55	0.775
7	tephriphonolite	51.42	0.70	3.00	0.00	9.40	0.33	13.18	21.25	0.54	0.02	0.00	99.84	0.734
7		50.69	0.66	3.12	0.00	9.44	0.40	13.24	21.92	0.58	0.03	0.00	100.08	0.788
3	trachyte	51.98	0.45	2.11	0.00	8.98	0.49	13.40	22.25	0.52	0.01	0.00	100.19	0.768
3		51.42	0.52	3.08	0.00	8.06	0.41	13.81	22.55	0.47	0.01	0.00	100.33	0.808
3		51.42	0.60	3.09	0.00	8.09	0.39	13.67	22.32	0.52	0.02	0.00	100.12	0.797
3		51.89	0.38	1.77	0.00	10.76	0.70	12.49	22.14	0.52	0.03	0.00	100.68	0.722
3		51.43	0.56	3.12	0.01	8.06	0.38	13.67	22.80	0.49	0.02	0.00	100.54	0.809

Sample	Rock	Si	Ti	Al^{IV}	Al^{VI}	Cr	Fe^{2+}	Fe^{3+}	Mn	Mg	Ca	Na	K	Ni	Sum
8	trachybasalt	1.875	0.028	0.125	0.039	0.001	0.236	0.074	0.010	0.717	0.850	0.045	0.000	0.000	4.000
8		1.886	0.024	0.114	0.046	0.002	0.242	0.058	0.009	0.727	0.853	0.039	0.001	0.000	3.999
8		1.861	0.023	0.139	0.043	0.000	0.220	0.089	0.009	0.715	0.859	0.040	0.001	0.000	3.999
8		1.880	0.022	0.120	0.048	0.000	0.227	0.068	0.009	0.735	0.851	0.039	0.001	0.000	3.999
8		1.850	0.031	0.150	0.062	0.000	0.241	0.066	0.010	0.693	0.857	0.039	0.001	0.000	3.999
9	trachybasalt	1.872	0.025	0.128	0.062	0.001	0.255	0.053	0.009	0.707	0.847	0.039	0.000	0.000	4.000
9		1.870	0.025	0.130	0.051	0.001	0.223	0.069	0.009	0.718	0.865	0.039	0.000	0.000	4.000
9		1.852	0.026	0.148	0.053	0.000	0.218	0.076	0.009	0.709	0.873	0.033	0.002	0.000	3.998
9		1.869	0.028	0.131	0.046	0.000	0.232	0.059	0.009	0.723	0.871	0.031	0.000	0.000	4.000
11	tephriphonolite	1.816	0.030	0.184	0.074	0.000	0.198	0.091	0.009	0.701	0.856	0.040	0.000	0.001	4.000
11		1.825	0.030	0.175	0.072	0.000	0.203	0.090	0.009	0.699	0.849	0.047	0.001	0.000	3.999
7	tephriphonolite	1.920	0.020	0.080	0.052	0.000	0.266	0.028	0.010	0.734	0.850	0.039	0.001	0.000	3.999
7		1.886	0.018	0.114	0.023	0.000	0.198	0.096	0.013	0.735	0.874	0.042	0.001	0.000	3.999
3	trachyte	1.933	0.013	0.067	0.025	0.000	0.225	0.054	0.015	0.743	0.887	0.037	0.000	0.000	4.000
3		1.901	0.014	0.099	0.035	0.000	0.181	0.069	0.013	0.761	0.893	0.034	0.000	0.000	4.000
3		1.906	0.017	0.094	0.040	0.000	0.192	0.058	0.012	0.755	0.886	0.037	0.001	0.000	3.999
3		1.935	0.011	0.065	0.013	0.000	0.267	0.069	0.022	0.695	0.885	0.038	0.001	0.000	3.999
3		1.898	0.016	0.102	0.034	0.000	0.177	0.072	0.012	0.752	0.902	0.035	0.001	0.000	3.999

Table 6. Continued.

Sample	Rock	Li	B	Sc	V	Cr	Co	Ni	Rb	Sr	Y	Zr	Nb	Ba	
8	trachybasalt	24.89	20.72	126.89	390.15	33.86	43.99	27.95	0.00	66.83	45.73	122.18	0.33	0.32	
8		24.88	16.76	122.91	381.46	19.33	43.51	29.74	0.00	88.74	44.43	124.34	0.38	22.71	
8		22.34	16.52	115.35	366.43	35.85	43.62	29.49	0.00	69.28	43.26	112.78	0.32	0.31	
8		25.16	35.46	120.68	384.67	11.54	43.97	25.24	5.40	95.91	46.62	138.60	0.48	23.96	
8		22.30	30.20	113.17	332.78	11.85	43.24	24.14	0.00	70.24	37.80	102.44	0.32	6.77	
9	trachybasalt	3.43	9.90	94.53	403.97	33.53	47.73	32.97	0.00	71.84	42.42	114.42	0.32	0.32	
9		3.15	8.50	111.68	436.53	25.69	48.25	35.56	0.00	80.59	39.36	119.87	0.32	0.36	
9		2.87	6.89	120.22	417.66	25.70	44.61	34.35	0.00	82.37	42.67	136.89	0.33	0.34	
9		2.65	8.02	130.69	431.00	9.16	45.55	27.21	0.00	75.14	45.62	139.02	0.36	0.38	
11	tephriphonolite	28.77	9.04	81.08	434.99	57.90	44.24	39.24	0.00	136.73	35.02	114.37	0.36	0.43	
11		29.53	9.44	92.95	489.54	39.71	44.39	36.14	0.00	129.06	37.39	128.58	0.40	0.49	
7	tephriphonolite	22.50	8.42	90.48	292.88	0.00	44.85	21.89	0.00	105.60	38.14	141.27	0.39	0.34	
7		22.08	8.26	92.20	295.97	6.20	44.26	21.61	0.00	107.35	38.57	143.82	0.40	0.31	
3	trachyte	35.74	6.36	86.76	127.53	0.00	28.04	0.71	0.00	63.37	57.24	146.51	0.35	0.27	
3		31.54	6.49	80.14	162.77	0.00	28.28	0.81	0.00	88.18	52.86	133.06	0.35	0.27	
3		36.86	6.43	78.24	163.71	0.00	29.77	1.14	0.00	103.69	50.09	123.73	0.32	0.28	
3		51.94	7.61	95.65	86.36	0.00	27.63	0.76	0.00	12.43	65.86	198.70	0.43	0.36	
3		33.89	5.68	78.53	150.48	0.00	27.96	1.37	0.00	94.51	47.69	114.00	0.32	0.26	

Sample	Rock	La	Ce	Pr	Nd	Sm	Eu	Gd	Tb	Dy	Ho	Er	Tm	Yb	Lu
8	trachybasalt	12.43	45.46	7.67	40.12	11.08	2.09	10.66	1.62	9.60	1.80	4.76	0.63	4.38	0.64
8		12.83	45.94	7.75	40.23	11.17	2.17	10.47	1.56	9.34	1.76	4.59	0.66	4.34	0.60
8		11.95	43.14	7.36	38.23	10.55	1.99	10.07	1.47	9.30	1.68	4.49	0.62	4.18	0.59
8		62.08	131.91	14.76	60.41	13.16	2.29	11.47	1.69	9.95	1.87	4.75	0.68	4.43	0.63
8		10.84	39.07	6.54	33.59	9.70	1.86	9.14	1.32	7.93	1.47	3.93	0.55	3.68	0.51
9	trachybasalt	11.63	44.82	7.62	40.00	11.23	2.25	10.93	1.48	9.49	1.67	4.44	0.60	4.07	0.54
9		11.44	42.75	7.39	38.83	10.82	2.22	9.96	1.39	8.64	1.51	3.99	0.56	3.79	0.51
9		12.15	44.62	7.76	41.21	11.53	2.34	11.01	1.64	9.30	1.65	4.31	0.59	3.91	0.56
9		12.17	44.67	7.81	42.57	12.01	2.40	11.48	1.72	9.82	1.77	4.69	0.64	4.07	0.59
11	tephriphonolite	12.75	48.57	8.17	40.96	11.24	2.35	9.74	1.33	7.70	1.41	3.54	0.48	2.93	0.39
11		13.84	52.34	8.75	44.76	11.89	2.55	10.31	1.43	8.25	1.44	3.71	0.49	3.21	0.44
7	tephriphonolite	13.64	50.38	8.33	41.66	11.13	2.32	9.74	1.40	8.23	1.51	3.96	0.53	3.65	0.52
7		13.90	50.80	8.15	41.48	11.39	2.34	9.73	1.39	8.34	1.50	3.88	0.54	3.51	0.50
3	trachyte	17.07	64.65	10.88	55.42	15.34	2.89	13.70	2.03	12.15	2.22	6.07	0.84	5.70	0.82
3		16.01	62.40	10.36	51.56	14.03	3.11	13.02	1.92	11.33	2.09	5.47	0.78	5.00	0.71
3		14.74	58.19	9.74	48.42	13.42	3.05	12.16	1.80	10.64	1.98	5.21	0.70	4.75	0.67
3		22.40	88.33	14.28	68.31	17.89	1.49	15.83	2.33	13.97	2.56	7.06	1.06	7.45	1.12
3		14.41	57.25	9.55	47.51	12.95	3.10	11.86	1.69	10.28	1.83	4.71	0.70	4.53	0.67

Table 6. Continued.

Sample	Rock	Hf	Ta	Pb	Th	U
8	trachybasalt	4.96	0.05	0.71	0.54	0.13
8		4.87	0.06	0.85	0.67	0.16
8		4.53	0.05	0.69	0.53	0.13
8		5.80	0.08	1.31	5.90	1.42
8		4.16	0.04	0.62	0.58	0.16
9	trachybasalt	4.76	0.05	0.83	0.55	0.12
9		5.03	0.06	0.73	0.52	0.12
9		5.97	0.06	0.72	0.61	0.11
9		6.09	0.07	0.70	0.64	0.12
11	tephriphonolite	4.61	0.06	0.81	0.68	0.15
11		5.47	0.07	0.89	0.77	0.17
7	tephriphonolite	5.46	0.07	0.64	0.59	0.12
7		5.54	0.07	0.69	0.62	0.14
3	trachyte	6.12	0.06	0.67	0.39	0.09
3		5.76	0.06	0.62	0.39	0.10
3		5.08	0.06	0.60	0.40	0.09
3		8.21	0.07	0.87	0.37	0.10
3		4.64	0.05	0.65	0.34	0.08

One of the most important features of the shoshonitic series is its K_2O/Na_2O ratio, which may exceed 1. This is also seen in numerous rocks in this study. On a (K_2O/Na_2O)–SiO_2 diagram (Figure 7g), they concentrate close to the limit where K_2O/Na_2O = 1.5. All samples, except some trachybasalts and an analcime-bearing tephriphonolite, plotted below the K_2O/Na_2O = 1 line.

REE profiles of the Qaleh-Khargooshi area shoshonites are shown in Figure 8. Chondrite-normalized REE patterns of all samples (Figure 8a) show a negative slope for LREE and a horizontal trace for the HREE. The HREE have more variations than the LREE. This diagram shows that all samples are much more enriched in REE than chondrites. Plotting the different rock units on the individual chondrite-normalized diagram reveals that trachybasalts, tephriphonolites and trachytes have similar REE patterns (Figure 8b, c). Trachydacites and the post-shoshonite granite have a negative Eu anomaly, but otherwise with the same REE patterns (Figure 8d).

Chemical data show that the trachydacites and the post-shoshonite granite have the same major and trace element contents. Normalizing the trachydacites against the post shoshonite granite confirms this and reveals that the last erupted trachydacite, is very similar to the post-shoshonite granite in REE content (Figure 8e, f). Normalizing all the samples against the REE contents of the manually separated matrix of trachydacite (Mat1), shows that Mat1 has similar REE contents to the trachytes (Figure 8g, h).

Harker diagrams (SiO_2-element) for the whole rock analyses shows that TiO_2, Al_2O_3, Fe_2O_3*, MnO, MgO, CaO, Co, Ba and Sr contents decrease with increasing SiO_2 content (Figure 9), but Na_2O contents vary little and present a nearly horizontal trend. The two analcime-bearing tephriphonolites have higher contents of Na_2O, as shown on the diagram (Figure 9g). On Sr and Ba Harker diagrams, two trachytes with big plagioclase and sanidine phenocrysts plot above the other samples (Figure 9i, j).

On K_2O, Rb, Cs, Zr, U, Th, Ta, Hf and Sc Harker diagrams, with increasing SiO_2 contents, the values of these elements drastically change direction around 60% SiO_2 (Figure 10). On a Cs Harker diagram, analcime-bearing tephriphonolites are enriched in Cs. Other samples show a similar Cs trend to that of other elements.

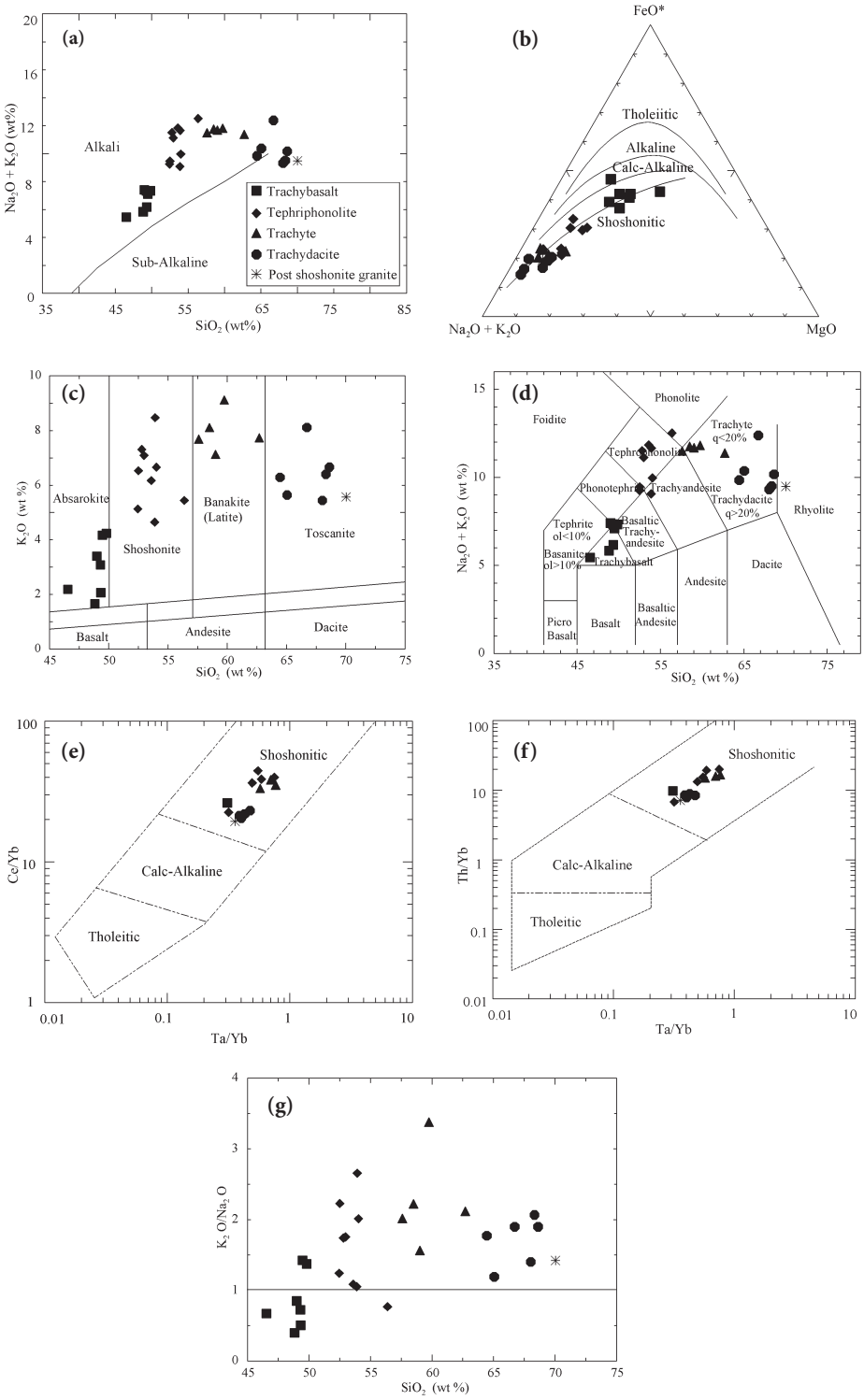

Figure 7. Different geochemical diagrams to identify the magmatic series, and rock classification based on the major and trace elements contents. **(a)** SiO_2-(Na_2O+K_2O) diagram from (Irvine & Baragar 1971); **(b)** AFM triangle from (Wimmenauer 1985); **(c)** SiO_2-K_2O diagram for classification of shoshonitic rock suites (McKenzie & Chappell 1972); **(d)** IUGS classification of rocks based on the TAS (Total Alkalis versus Silica) diagram (Le Maitre *et al.* 2005); **(e, f)** Ta/Yb-Ce/Yb and Ta/Yb-Th/Yb diagrams (Pearce 1982); **(g)** SiO_2-(K_2O/Na_2O) diagram and position of analyzed rocks.

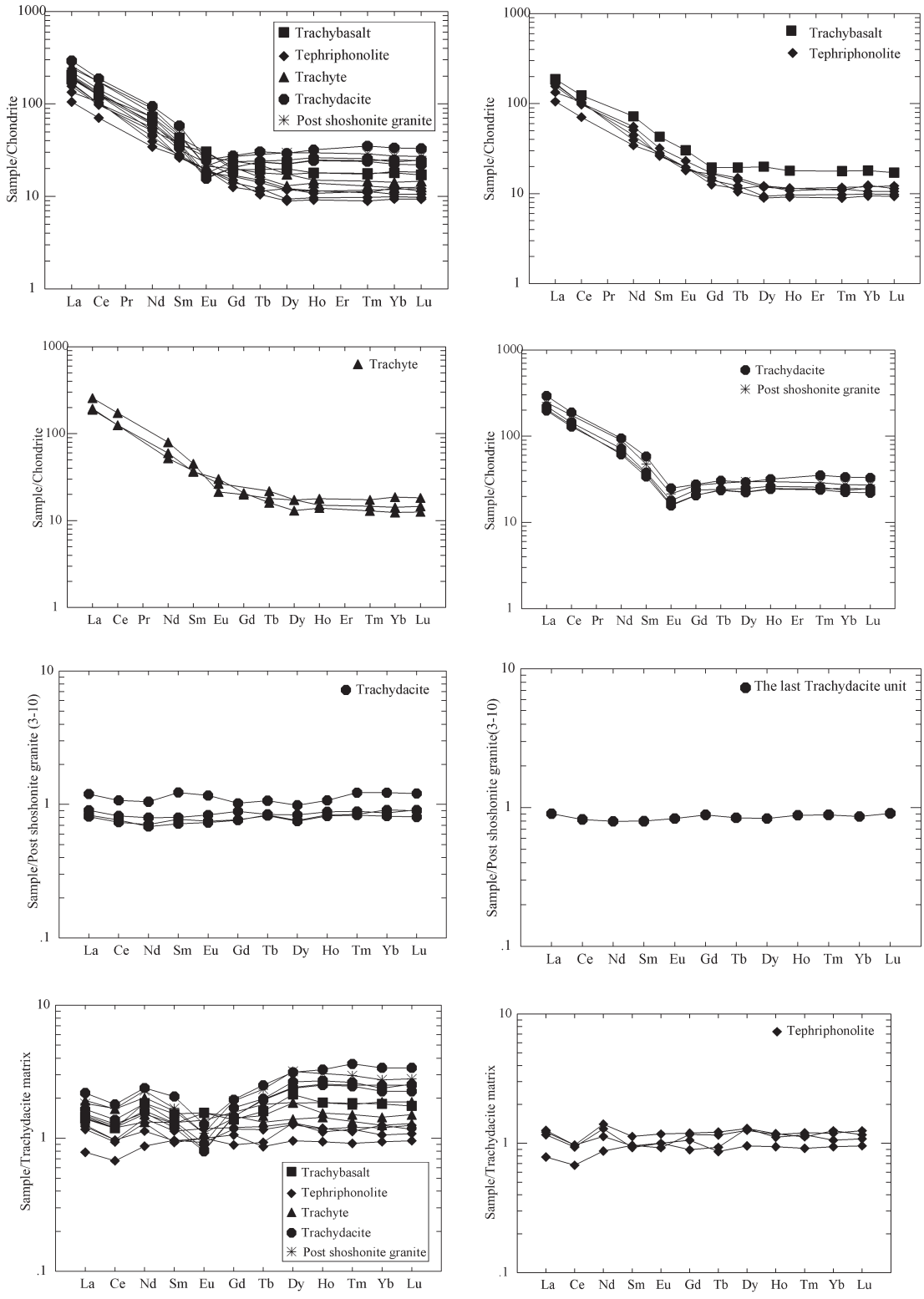

Figure 8. Different spider diagrams based on the REE contents for all studied rock units.

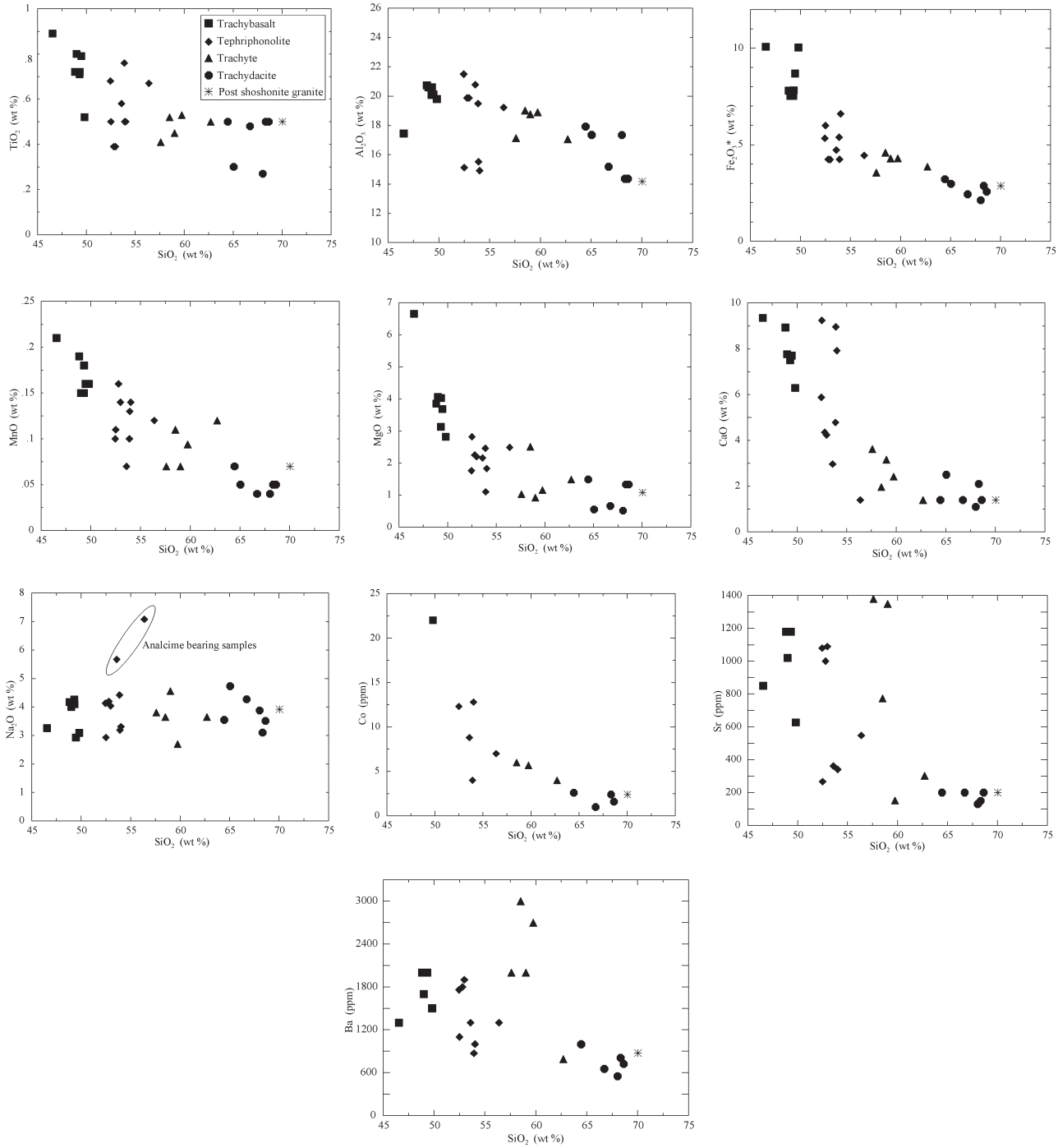

Figure 9. SiO_2-element (Harker) diagrams for whole rock analyzed samples.

Mineral Chemistry

Clinopyroxene is present as phenocrysts in trachybasalt, tephriphonolite and trachyte and occurs in the groundmass of all members of the shoshonite association. Clinopyroxenes in trachydacites are small and altered.

Clinopyroxenes are rich in calcium and magnesium and exhibit almost no iron enrichment,

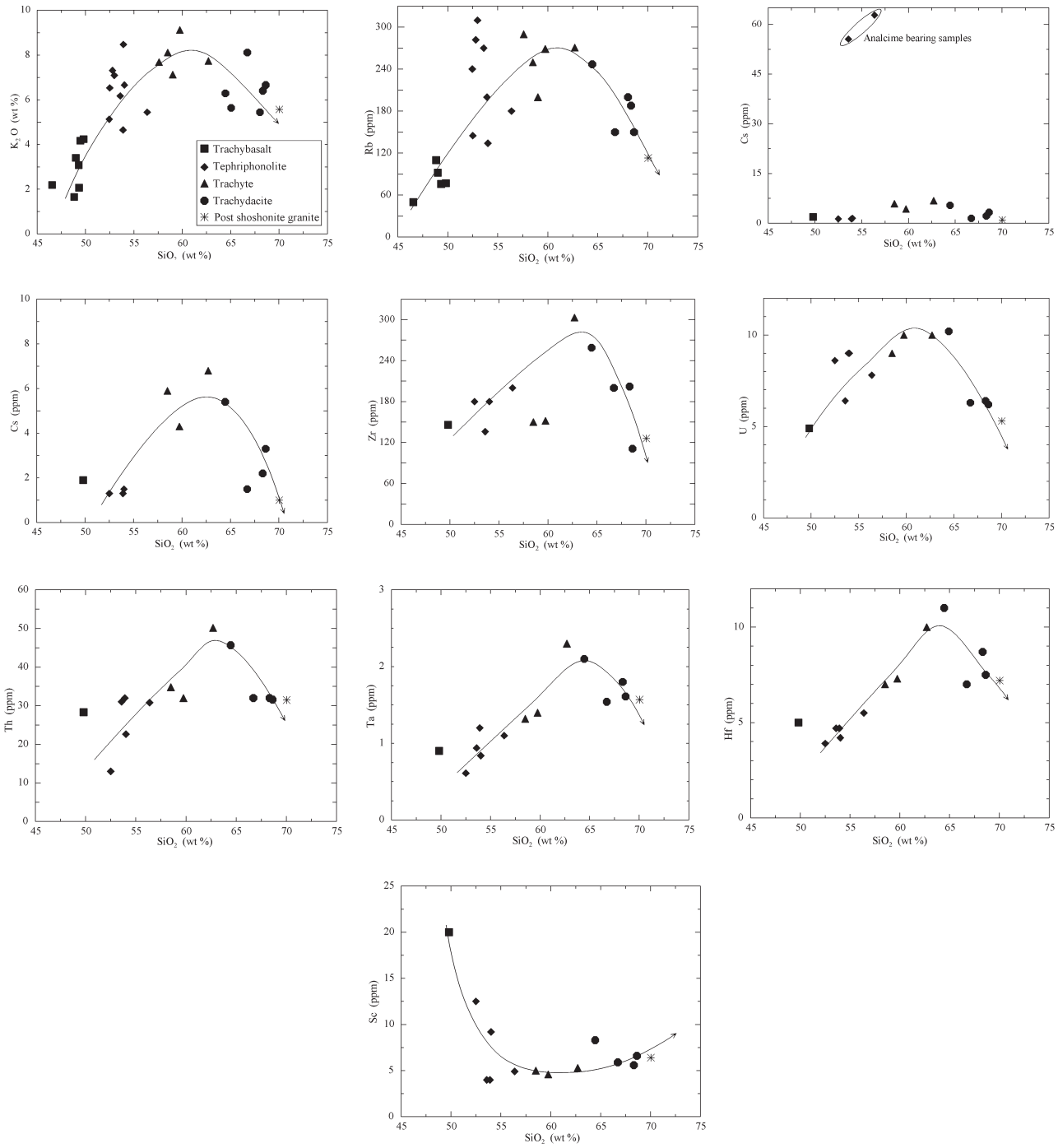

Figure 10. Drastic direction change in abundance of some elements in SiO_2-element diagrams near 60 wt% SiO_2.

and thus differ from those of the tholeites and alkali basalts. Figure 11 shows that, irrespective of the composition of the host rocks in which they occur, the clinopyroxenes tend to cluster in diopside field. In tholeites and alkali basalts, the composition of clinopyroxenes is strung out along a differentiation curve. Clinopyroxenes from Qaleh-Khargooshi shoshonitic members are diopsides.

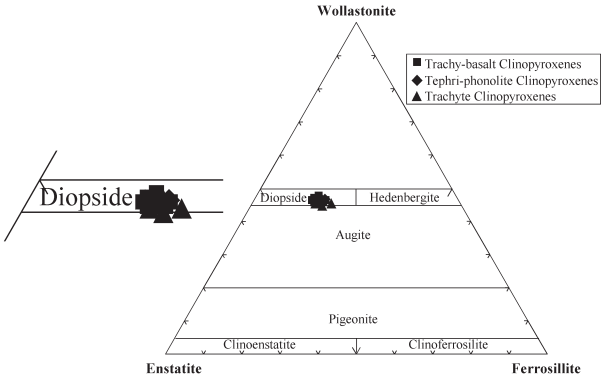

Figure 11. Clinopyroxenes from the Qaleh-Khargooshi shoshonites plotted in the pyroxene triangle. The enlarged diopside field is shown at left.

The Mg#-element graphs (Figure 12) show a differentiation in the composition of pyroxenes, but scattering of pyroxenes with same symbols in these diagrams and the distribution of different rock units (identified by different symbols), reveals that clinopyroxenes have a range of compositions in each rock unit.

Trace elements in clinopyroxene (Table 6) are very sensitive indicators of the processes involved in its formation. All analyzed clinopyroxenes are highly enriched in light REE and show similar concave-upward chondrite-normalized patterns (Sun & McDonough 1989) (Figure 13). Ce/Yb ratios range from 10 to 30. These features are comparable with clinopyroxenes in alkali basalts (Wang & Gasparik 2001).

The chondrite normalized REE patterns of clinopyroxenes reveal that most of the studied clinopyroxenes have the same REE trend, are enriched in LREE, and have a negative Eu anomaly. The latter can result from the partly simultaneous crystallization of plagioclase and clinopyroxene in the shoshonitic melts. The preferential partitioning of Eu^{2+} in plagioclase causes a negative Eu anomaly to develop in coexisting melt and clinopyroxene. One of the trachybasalt clinopyroxenes is more enriched in LREE than the others. It may have crystallized before than the other clinopyroxens. Sub-parallel REE patterns of clinopyroxenes in this shoshonitic suite suggests fractional crystallization and identical petrogenesis of the analyzed clinopyroxenes.

Comparison of the average clinopyroxene composition in each rock unit shows that the tephriphonolite clinopyroxenes have the lowest REE contents and the trachyte clinopyroxenes have the highest REE abundance. This characteristic demonstrates that the average REE contents in these clinopyroxenes do not follow the normal crystallization trend. In normal crstallization, the trachybasalt clinopyroxenes should have the lowest REE contents. Therefore this indicates the complex crystallization of the primary magma.

Figure 14 shows trace element contents of clinopyroxenes normalized to primitive mantle (Sun & McDonough 1989). It illustrates that Cr, Ni, Co and Nb contents are lower than in the primitive mantle, and Eu, Zr, Sr, Pb, U, Th, Ta, Ti and Nb have negative anomalies.

Plagioclase is present in all rock units. Plagioclase in trachybasalts is labradorite and is albite in trachydacites. Albites produced from analcimes and clinopyroxenes, have the same composition and are near to an ideal formula.

K-feldspars are sanidine and anorthoclase, and present in all shoshonitic members. Some sanidine crystals in trachytes are rimmed by another phase of sanidine with higher K_2O and lower Na_2O.

Analcime is present as phenocrysts in trachybasalt and especially in tephriphonolite. The analyzed analcimes are almost homogenous in chemical composition. The maximum content of CaO in analcimes is 1.03% in trachybasalt.

Analcime may occur in a variety of geological setting (Prelevié *et al.* 2004). Different investigations into the origin of analcime describe its mineralogical complexity and wide range of formation temperatures. Petrologically and geochemically, the most interesting debate is about its primary (magmatic) or secondary (transformation) origin. Petrography, mineral chemistry and SEM studies reveal that all analcimes in the studied shoshonitic succession were produced by Na-metasomatism of leucite crystals. A non-magmatic origin for these analcimes is deduced because:

(1) Cracks in analcimes result from a volume increase of about 10% during the transformation of leucite to analcime (Karlsson & Clayton 1991; Putnis *et al.* 1994).

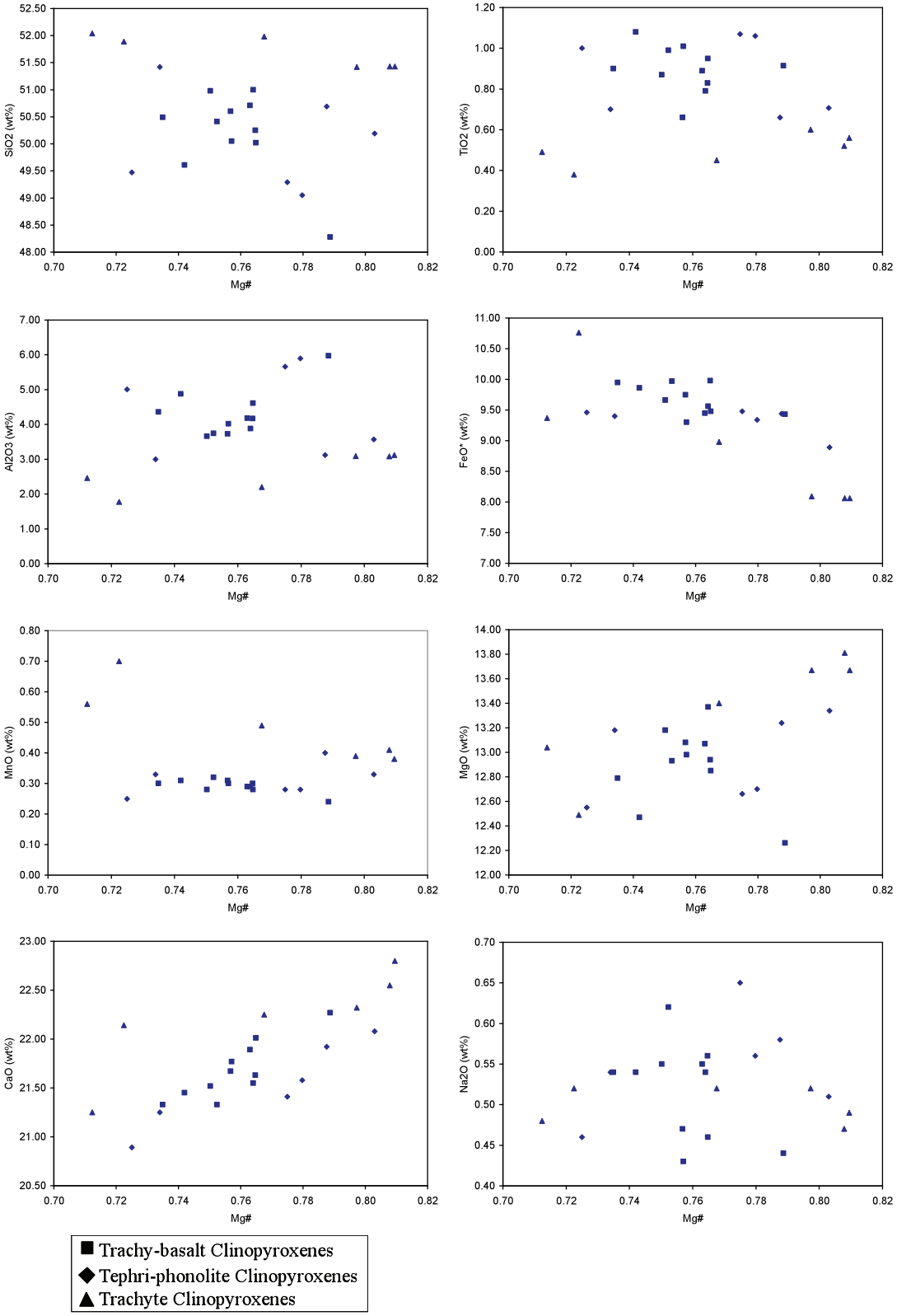

Figure 12. Diagrams of Mg# versus element oxides for clinopyroxenes of the Qaleh-Khargooshi area shoshonitic association.

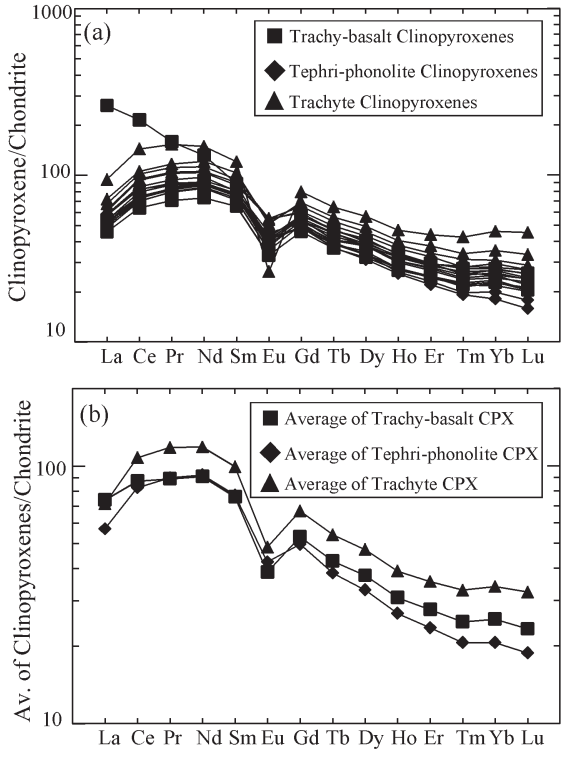

Figure 13. **(a)** Chondrite normalized REE contents of clinopyroxenes; **(b)** average clinopyroxene compositions in different rock units are normalized to chondrite.

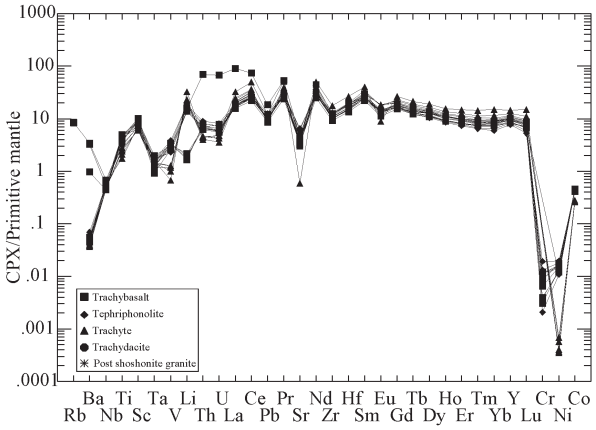

Figure 14. Abundance of trace elements in clinopyroxenes normalized to primitive mantle (Sun & McDonough 1989).

(2) The analcime crystals preserve the macroscopic morphology of the leucite parent.

(3) Potassium released by the leucite to analcime reaction, caused the growth of the potassic rim around the feldspars (anti-rapakivi texture). The studied analcimes are thus the result of an ion-exchange reaction at subsolidus temperatures (Putnis *et al.* 1994, 2007):

$$\text{Leucite} + Na^+ + H_2O = \text{Analcime} + K^+$$

$$KAlSi_2O_6 + Na^+ + H_2O = NaAlSi_2O_6.H_2O + K^+$$

In analcime the H_2O molecules occupy the structural channels occupied by K in leucite, while the Na occupies smaller interconnecting channels which are empty in leucite (Gottardi & Galli 1985). The resulting potassic fluids induce growth of the potassic rim of plagioclases and sanidines. Observations of partially transformed leucite are rare, presumably due to the rapid reaction rate (Putnis *et al.* 1994).

(4) Absence of other hydrous minerals in the petrographic study, the homogeneous composition of analcimes, and the absence of primary magmatic sodic-mineral such as Na-pyroxene, are other reasons for deducing a non-magmatic origin of the analcimes.

(5) SEM and thermal analysis of analcimes (including DTA, TG, DTG, and DSC) (Giampaolo & Lombardi 1994; Putnis *et al.* 1994) concluded that the analcimes of study area are X-type (secondary) analcimes.

(6) The analyzed samples containing large crystals of analcime have very considerable amounts of Cs and Rb that may be attributed to the original substitution of K in leucite structure.

Petrogenesis

Scarce, but widely distributed potassium-rich rocks are found in several tectonic environments, such as continental cratons, post-collisional areas, active orogenic belts, and, to a lesser extent, oceanic intraplate settings. Shoshonitic rocks are associated with many continental and oceanic arcs (Peccerillo 1992) and their petrogenesis has been discussed (Foley & Peccerillo 1992; Jiang *et al.* 2002; Conceição & Green 2004; Gill *et al.* 2004; Prelevié *et al.* 2004; Eklund & Shebanov 2005).

The most important processes proposed for melt generation in subduction zones are: (1)

decompression melting due to crustal flow and/or extension (Elkins-Tanton *et al.* 2001) and (2) melting due to hydrous metasomatism of the mantle wedge above the subducting slab (Gill 1981). If decompression melting occurs during mantle flow into the mantle wedge, it may leave behind a depleted potentially harzburgitic mantle that will be subsequently metasomatized by a slab component (Hesse & Grove 2003). Potassium, sodium, and silica are the major elements that are most strongly enriched in the metasomatic agent or a slab melt (Rapp *et al.* 1999; Rose *et al.* 2001). Calc-alkaline, and especially highly potassic volcanic rocks such as lamprophyres and members of the Absarokite-Shoshonite-Banakite series, have been interpreted as partial melts of the metasomatized/veined peridotitic mantle (Tatsumi & Koyaguchi 1989). Luhr (1997) concluded that the highly potassic volcanic rocks in western Mexico represent 'the geochemical essence of subduction zone magmatism'. Absarokites are amongst the most primitive of these potassic volcanic rocks (Hesse & Grove 2003). The primary magma should pass through the continental crust during its ascent to the earth's surface. Depending on thickness of the continental crust, some magmas derived from the sub-continental mantle do not reach the surface in pristine condition. Susceptibility of mantle-derived magmas to contamination by continental crust was recognized many years ago in field, petrography, geochemical and isotopic studies (e.g., Watson 1982; Pe-Piper *et al.* 2003).

Shoshonitic lavas are associated with regions that were incompletely or only recently tectonically stabilized at the time of their extrusion (Joplin *et al.* 1972). This fits their geographical distribution in the Urumieh-Dokhtar volcanic arc. Subduction of Neothethys oceanic crust was completed in the Upper Eocene to Early Oligocene (30–35 Ma) (Agard *et al.* 2005; Omrani *et al.* 2008) and the age of this shoshonitic association is Late Eocene.

The study of chondrite-normalized REE patterns of these rocks and the high concentrations of LREE and high La/Lu ratios observed in these shoshonites suggest a small degree of partial melting of a mantle source. Figure 15a, b show that the Qaleh-Khargooshi shoshonites relate to an enriched mantle and most samples are metaluminous.

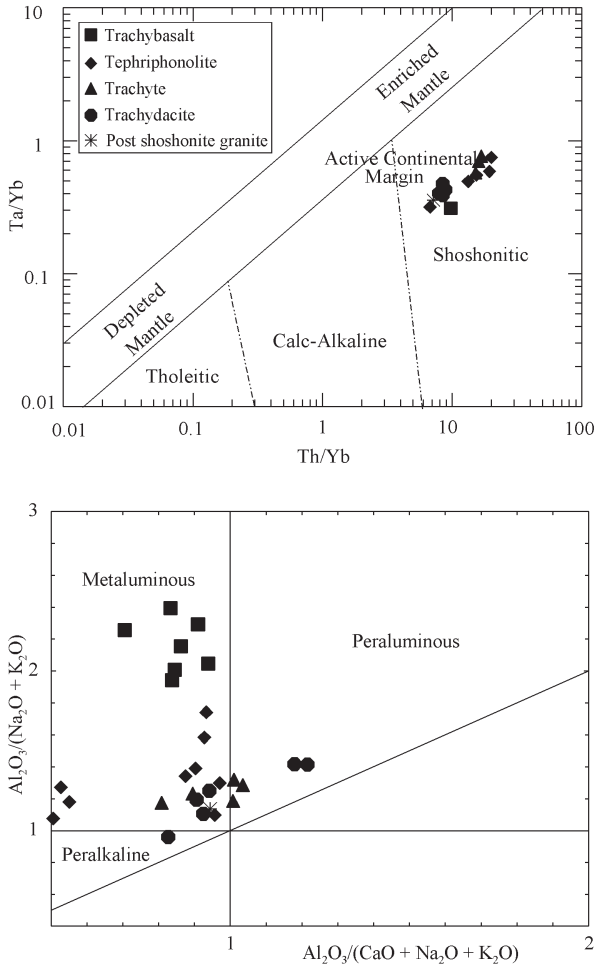

Figure 15. Th/Yb-Ta/Yb (Pearce 1982) and aluminum saturation index (Maniar & Piccoli 1989) diagrams for the studied rocks.

The high K_2O (up to 9.12 wt%), considerable MgO values (up to 6.66 wt%), high K_2O/Na_2O ratios and the trace elements signature might be attributed to enrichment processes in the mantle wedge above a subduction zone. Also, the high Rb and Ba contents in the Qaleh-Khargooshi shoshonitic rocks may indicate a repository mineral phase in the peridotite of the upper mantle wedge (Aftabi & Atapour 2000). The most likely mineral is therefore phlogopite, as suggested by Muller & Groves (2000) for many potassic rocks. This may be related to the melting of a phlogopite-bearing subducting plate or phlogopite peridotite, which produces an alkaline potassium-rich parent magma. Depletion in Ti is probably

related to residual titanian phases (titanite and rutile) in the hydrated mantle wedge, as was suggested by Foley & Wheller (1990).

Geological and whole rock geochemistry studies (Torabi 1997) concluded that the parent magma of shoshonitic rocks is originated by low degree of partial melting of a metasomatized enriched mantle source. During ascent through thick continental crust (42 km), the parent magma suffered the assimilation. Depending on the portion of continental crust in making the contaminated magma, different rock units of shoshonitic series will form.'

There is evidence of exchanges between the primary basaltic melt and continental crust in the field, petrography, minerals and whole rock chemistry:

(1) A wide chemical range of rock units from silica-undersaturated to highly silica-saturated rocks is present. In the Petrogenic Residua System, the basic silica-undersaturated primary magma can not pass the albite-orthoclase thermal barrier to formation of considerable masses of trachydacite. This range of rock chemistry cannot be explained by simple crystallization of a basic primary melt.

(2) Scattered basic magmatic inclusions are present in the trachytes and trachydacites.

(3) Based on the log-log plot of compatible and incompatible elements (Yanagi & Yamashita 1994), simple crystallization is not responsible for the formation of the Qaleh-Khargooshi shoshonites: possibly mixing and contamination are other factors (Figure 16a, b).

(4) The petrography and whole rock chemistry of the trachydacites is similar to that of the post-shoshonite granite (Figures 7 & 8).

(5) The manually separated matrix of trachydacite is compositionally tephriphonolite (Figures 7 & 8).

(6) The drastic direction change of some elements (K_2O, Rb, Cs, Th, Ta, Hf, Sc, Zr and U) on the Harker diagrams near to 60% SiO_2, points to special phenomena that are not in agreement with simple crystallization effects.

(7) The Na_2O direction on the Harker diagram, shows that the Na_2O content of mantle-derived magma is buffered against the contamination by crustal materials: that agrees with Watson's (1982) findings.

(8) In the tephriphonolite unit, some clinopyroxenes are replaced pseudomorphously by albite. In some cases the replacement is incomplete, and a symplectite of clinopyroxene and albite was observed.

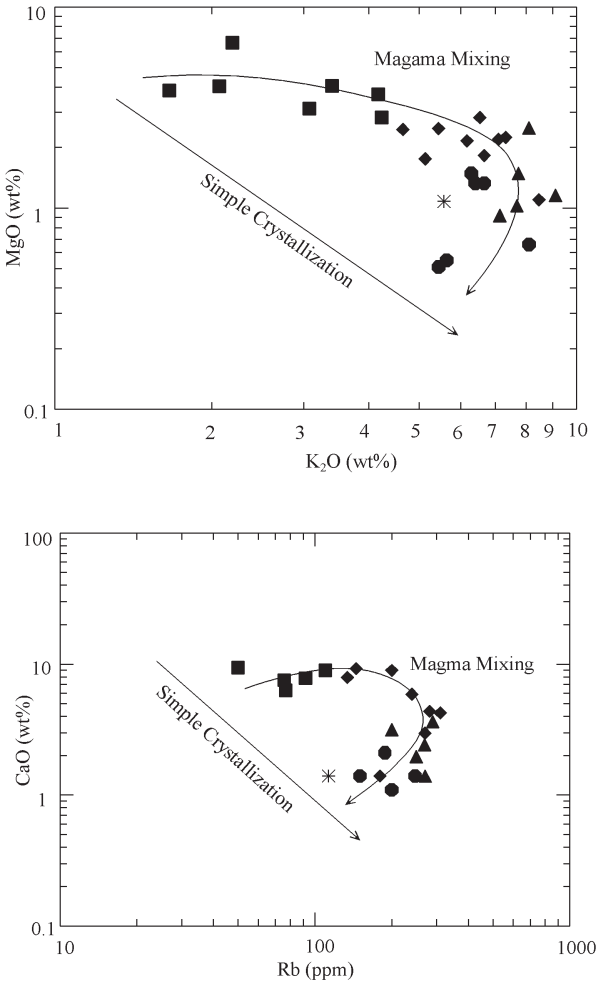

Figure 16. Curvature of analyzed samples from basic to acid in log-log plot incompatible-compatible elements diagrams from Yanagi & Yamashita (1994).

(9) In some tephriphonolites, analcimes are pseudomorphously replaced by albite, according to the reaction:

$$NaAlSi_2O_6.(H_2O) + SiO_2 = NaAlSi_3O_8 + H_2O$$

SiO_2 increase and H_2O decrease occurred in this reaction.

(10) In tephriphonolites and trachytes, the sanidine is partly altered to albite and anorthoclase, according to the reaction:

$$\text{Sanidine} + Na^+ = \text{Albite} + K^+$$

$$KAlSi_3O_8 + Na^+ = NaAlSi_3O_8 + K^+$$

The resulting potassic fluids produced the observed potassic rim of plagioclases and sanidines. The last three reactions show, after changing of all leucites to analcime (because of rapid kinetics), the fluids follow the other minerals (as clinopyroxene, analcime and sanidine) to changing.

(11) The morphology or habit of plagioclase is different in all rock units of the studied shoshonite. The shape of plagioclase ranges from tabular in trachybasalt to skeletal in tephriphonolite, dendritic in trachyte, and spongy and radial (spherulitic) in trachydacite; the latter is interpreted as consequence of undercooling processes (Lofgren 1974; Fowler 1990). Lofgren (1974) has experimentally produced plagioclase with cellular morphology, finding that the growth of non-cellular (tabular), skeletal, dendritic, or spherulitic plagioclase is dependent on undercooling, increasing respectively over a range of about 250 °C. The undercooling may occur by heat loss to wallrock, mixing with relatively cool felsic magma or volcanic eruption.

(12) Anti-rapakivi texture was observed in trachybasalts and tephriphonolites, and is evidence of magma mixing and contamination (Eliston 1985). Mantling textures occur in hybrid rocks of magma mixing and contamination origin (Hibard 1981).

(13) Sanidines in trachytes and trachydacites display resorbtion or ovoidal structures, and have a dusty rim, interpreted as evidence of magma mixing and contamination (Wark & Stimac 1992). In magmas already containing some K-feldspar crystals, mixing with magma several hundred degrees hotter results in partial resorbtion and rounding of K-feldspar crystals.

(14) Quartz crystals in trachydacites have serrated boundaries, showing that they were not in equilibrium with the matrix.

(15) Clinopyroxene is present in all rock units and chemically different clinopyroxenes may coexist in the same rock unit. The average REE contents in the clinopyroxenes do not obey the crystallization trend.

Thus, different lines of evidence show that the Qaleh-Khargooshi shoshinitic rocks formed by contamination of a basaltic crystal mush rich in K, and raise the question as to whether magma mixing and contamination were the predominant processes in the evolution of the shoshonitic suite.

Geotectonic Setting

The studied rocks have high concentrations of LILE and REE, and, based on their geochemistry are similar to those of subduction or continental arc-related potassic rocks. Chondrite-normalized incompatible and rare earth element abundances reveal negative anomalies in Ti and Cr, compared to the remaining elements, and this is typical for potassic volcanic rocks of continental arcs or convergent margins (Muller & Groves 2000). Tectonomagmatic diagrams show that the Qaleh-Khargooshi shoshonites plot within the fields of subduction-related arc suites, destructive margins and continental arcs (Figure 17a–c). Foley (1992) classified the potassic and ultrapotassic magmas into three different groups: the Qaleh-Khargooshi shoshonites are similar to his Group III, which is related to active continental margins (Figure 17d–f).

Comprehensive studies of the tectonic evolution of the Central Iran microplate and its subsequent collision with Arabia are published (Alavi 1994; Agard *et al.* 2005; Omrani *et al.* 2008). The regional geology of Central Iran and the geological history of UDMA confirm the subduction-related tectonic regime that is suggested by theoretical data.

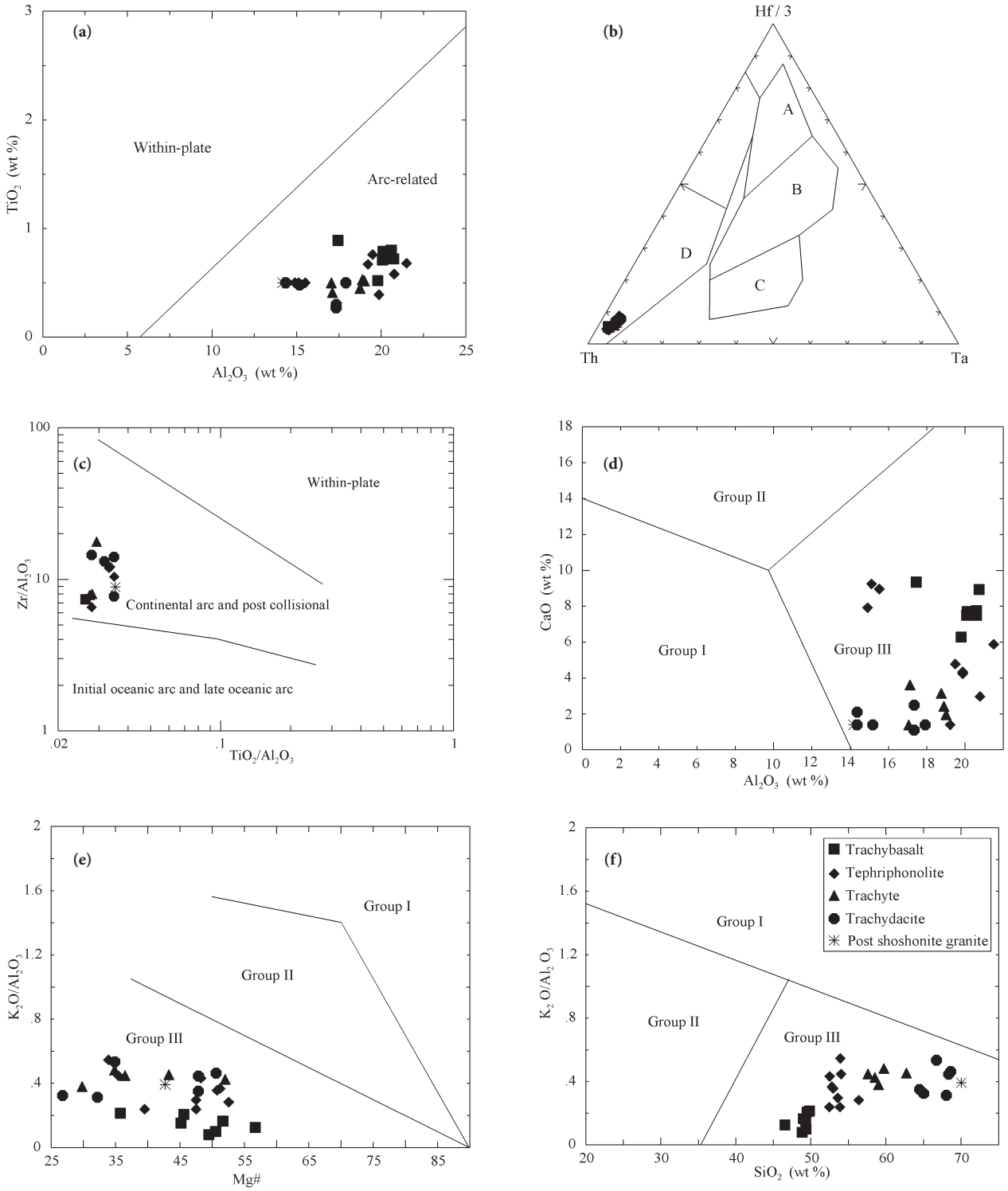

Figure 17. Geochemical tectonics discrimination diagrams for studied rocks. **(a)** Al_2O_3-TiO_2 diagram (Muller & Groves 2000); **(b)** Th-(Hf/3)-Ta ternary diagram (Wood 1980), D is the field of destructive margins; **(c)** (TiO_2/Al_2O_3)-(Zr/Al_2O_3) diagram (Muller *et al.* 1992); **(d–f)** diagrams based on the major elements used to discriminate between the different groups of potassic and ultrapotassic rocks (Foley 1992).

The enrichment of incompatible elements and high LREE/HREE ratios cannot be derived from a depleted mantle source via a single-stage melting process. Instead, a metasomatized mantle source is required. The enrichment in incompatible elements in this mantle source must have been sufficiently ancient to generate the observed chemistry of the studied rocks. For extensive subduction-related metasomatism of the mantle, considerable length of time is necessary (e.g., at least 24 million years in case of Greya *et al.* 2002). The Late Triassic to Late Eocene or Early Oligocene subduction of Neotethys in Iran (Agard *et al.* 2005; Omrani *et al.* 2008) is the cause of volatile enrichment of the mantle and shoshonitic magmatism in Upper Eocene. Enrichment of the mantle and metasomatism can be attributed to the former subduction, and contemporaneous subduction in Upper Eocene can be the cause of magmatism. Therefore, the former and contemporaneous subduction of Neotethys is the cause of the upper mantle deformation, metasomatism and shoshonitic volcanism in the Qaleh-Khargooshi area.

Conclusions

The volatile enrichment of sub-continental mantle of the UDMA, and Late Eocene shoshonitic magmatism along the UDMA was caused by former and contemporaneous Neotethys oceanic crust subduction. Mesozoic to Cenozoic subduction of the Neotethys oceanic crust was also able to generate mantle metasomatism and shoshonitic magmatism in Late Eocene.

The wide range of chemical composition in the Qaleh-Khargooshi shoshonites results from the crustal contamination and fractional crystallization of primary absarokitic magma during its ascent through thick continental crust, as shown by field studies, petrographic and geochemical evidence. By increasing the proportion of crustal contamination, different rocks from trachybasalt to trachydacite were formed. The crustal contamination thus has a very important role in making the UDMA shoshonites. Geochemically, these rocks are similar to potassic continental arc subduction related rocks.

Acknowledgements

The author thanks Professor Shoji Arai, Dr. Juergen Koepke and ENTC for laboratory facilities. The author express his thanks to Dr. Samuele Agostini who kindly examined the first version of the manuscript. Review of the manuscript by anonymous referees of the Turkish Journal of Earth Sciences is gratefully acknowledged. John A. Winchester edited the English of the final text.

References

Aftabi, A. & Atapour, H. 2000. Regional aspects of shoshonitic volcanism in Iran. *Episodes* **23**, 119–125.

Agard, P., Omrani, J., Jolivet, L. & Mouthereau, F. 2005. Convergence history across Zagros (Iran): constraints from collisional and earlier deformation. *International Journal of Earth Sciences* **94**, 401–419.

Alavi, M. 1994. Tectonics of the Zagros orogenic belt of Iran: New data and interpretations. *Tectonophysics* **229**, 211–238.

Amidi, S.M. 1977. *Etude géologique de la région de Natanz-Surk (Iran, Central).* Thèse Ph.D., Universita Grénoble, France.

Amidi, S.M., Emami, M.H. & Michel, R. 1984. Alkaline character of Eocene volcanism in the middle part of central Iran and its geodynamic situation. *International Journal of Earth Sciences* **73,** 917–932.

Conceição, R.V. & Green, D.H. 2004. Derivation of potassic (shoshonitic) magmas by decompression melting of phlogopite + pargasite lherzolite. *Lithos* **72**, 209–229.

Dehghani, G.A. & Markis, J. 1983. *The Gravity Field and Crustal Structure of Iran*. In geodynamic project (Geotraverse) in Iran, Geological survey of Iran, Report no. **51,** 51–68.

Eklund, O. & Shebanov, A. 2005. Prolonged postcollisional shoshonitic magmatism in the southern Svecofennian domain: a case study of the Åva granite–lamprophyre ring complex. *Lithos* **80**, 229–247.

Eliston, J.N. 1985. Rapakivi texture. *Earth Science Reviews* **22**, 1–92.

Elkins-Tanton, L.T., Grove, T.L. & Donnelly Nolan, J. 2001. Hot, shallow mantle melting under the Cascades volcanic arc. *Geology* **29**, 631–634.

Foley, S. 1992. Petrological characterization of the source components of potassic magmas, geochemical and experimental constraints. *Lithos* **28**, 187–204.

Foley, S.F. & Peccerillo, A. 1992. Potassic and ultrapotassic magmas and their origin. *Lithos* **28**, 181–185.

Foley, S.F. & Wheller, G.E. 1990. Parallels in the origin of the geochemical signature of island arc volcanic rocks and continental potassic igneous rocks: the role of titanites. *Chemical Geology* **85**, 1–18.

Fowler, A.D. 1990. Self-organized mineral textures of igneous rocks: the fractal approach. *Earth Sciences Reviews* **29**, 47–55**.**

Giampaolo, C. & Lombardi, G. 1994. Thermal behavior of analcimes from two different genetic environments. *European Journal of Mineralogy* **6**, 285–289.

Gill, J. 1981. *Orogenic Andesites and Plate Tectonics*. Springer-Verlag, New York.

Gill, R.C.O., Aparicio, A., El Azzouzi, M., Hernandez, J., Thirlwall, M.F., Bourgois, J. & Marriner, G.F. 2004. Depleted arc volcanism in the Alboran Sea and shoshonitic volcanism in Morocco: geochemical and isotopic constraints on Neogene tectonic processes. *Lithos* **78**, 363–388.

Gottardi, G. & Galli, E. 1985. *Natural Zeolites*. Springer-Verlag, Berlin.

Greya, T.V., Perchuk, L.L., Maresch, W.V., Willner, A.P., Van Reenen, D.D. & Smit, C.A. 2002. Thermal regime and gravitational instability of multi-layered continental crust: implications for the buoyant exhumation of high-grade metamorphic rocks. *European Journal of Mineralogy* **14**, 687–699.

Hesse, M. & Grove, T.L. 2003. Absarokites from the western Mexican volcanic belt: constraints on mantle wedge conditions. *Contributions to Mineralogy and Petrology* **146**, 10–27.

Hibard, M.J. 1981. The magma mixing origin of mantled feldspars. *Contributions to Mineralogy and Petrology* **76**, 158–170.

Iddings, J.P. 1895. Absarokite-shoshonite-banakite series. *Journal of Geology* **3**, 935–959.

Irvine, T.N. & Baragar, W.R.A. 1971. A guide to the chemical classification of the common volcanic rocks. *Canadian Journal of Earth Sciences* **8**, 523–548.

Jiang Y.H., Jiang, Sh.Y., Ling, H.F., Zhou, X.R., Rui, X.J. & Yang, W.Zh. 2002. Petrology and geochemistry of shoshonitic plutons from the western Kunlun orogenic belt, Xinjiang, northwestern China: implications for granitoid geneses. *Lithos* **63**, 165–187.

Joplin, G.A. 1965. The problem of the potash-rich basaltic rocks. *Mineralogical Magazine* **34**, 266–275.

Joplin, G.A., Kiss, E., Ware, N.H. & Widdowson, J.R. 1972. Some chemical data on members of the shoshonite association. *Mineralogical Magazine* **38**, 936–945.

Karlsson, H.R. & Clayton, R.N. 1991. Analcime phenocrysts in igneous rocks: primary or secondary? *American Mineralogist* **76**, 189–199.

Le Maitre, R.W., Streckeisen, A., Zanettin, B. & Le Bas, M.J. 2005. *Igneous Rocks: A Classification and Glossary of Terms: Recommendations of the International Union of Geological Sciences Subcommission on the Systematics of Igneous Rocks.* 2nd edition, Cambridge University press, Cambridge.

Lofgren, G. 1974. An experimental study of plagioclase crystal morphology: isothermal crystallization. *American Journal of Science* **274**, 243–273.

Luhr, J.F. 1997. Extensional tectonics and the diverse primitive volcanic rocks in the western Mexican Volcanic Belt. *Canadian Mineralogist* **35**, 473–500.

Maniar, P.D. & Piccoli, P.M. 1989. Tectonic discrimination of granitoids. *Geological Society of American Bulletin* **101**, 635–643.

McKenzie, D.E. & Chappell, B.W. 1972. Shoshonite and calc-alkaline lavas from the highlands of. Papua New Guinea. *Contributions to Mineralogy and Petrology* **35**, 50–62.

Mehdizadeh, H., Liotard, J.M. & Dautria, J.M. 2002. Geochemical characteristics of an intracontinental shoshonitic association: the example of the Damavand volcano, Iran. *Comptes Rendus Geosciences* **334**, 111–117.

Muller, D. & Groves, D.I. 2000. *Potassic Igneous Rocks and Associated Gold-copper Mineralization*. Springer-Verlag., New York.

Muller, D., Rock, N.M.S. & Groves, D.I. 1992. Geochemical discrimination between shoshonitic and potassic volcanic rocks in different tectonic settings: a pilot study. *Mineralogy and Petrology* **46**, 259–289.

Omrani, J., Agard, P., Whitechurch, H., Benoit, M., Prouteau, G. & Jolivet, L. 2008. Arc-magmatism and subduction history beneath the Zagros Mountains, Iran: a new report of adakites and geodynamic consequences. *Lithos* **106**, 380–398.

Pearce, J.A. 1982. Trace element characteristics of lavas from destructive plate boundaries. *In*: Thorpe, R.S. (ed), *Andesites: Orogenic Andesites and Related Rocks*. John Wiley & Sons, Chichester, 525–548.

Pecccerillo, A. 1992. Potassic and ultrapotassic rocks: compositional characteristics, petrogenesis, and geologic significance. *Episodes* **15**, 243–251.

Peccerillo, A. & Taylor, S.R. 1976. Geochemistry of Eocene calc-alkaline volcanic-rocks from Kastamonu area, northern Turkey. *Contributions to Mineralogy and Petrology* **58**, 63–81.

Pe-Piper, G., Matarangas, D., Reynolds, P.H. & Chatterjee, A.K. 2003. Shoshonites from Agios Nectarios, Lesbos, Greece: origin by mixing of felsic and mafic magma. *European Journal of Mineralogy* **15**, 117–125.

Prelević, D., Foley, S.F., Cvetković**,** V. & Romer, R.L. 2004. The analcime problem and its impact on the geochemistry of ultrapotassic rocks from Serbia. *Mineralogical Magazine* **68**, 633–648.

Putnis, A., Putnis, C.V. & Giampaolo, C. 1994. The microtexture of analcime phenocrysts in igneous rocks. *European Journal of Mineralogy* **6**, 627–632.

Putnis, C.V., Geisler, T., Schmid-Beurmann, P., Stephan, T. & Giampaolo, C. 2007. An experimental study of the replacement of leucite by analcime. *American Mineralogist* **92**, 19–26.

Rapp, R.P., Shimizu, N., Norman, M.D. & Applegate, G.S. 1999. Reaction between slab-derived melts and peridotite in the mantle wedge: experimental constraints at 3.8 GPa. *Chemical Geology* **160**, 335–356.

Rose, E.F., Shimizu, N., Layne, G.D. & Grove, T.L. 2001. Melt production beneath Mt Shasta from boron data in primitive melt inclusions. *Science* **293**, 281–283.

Sun, S.S. & McDonough, W.F. 1989. Chemical and isotopic systematics of oceanic basalts: implications for mantle Composition and Processes. *In*: Saunders, A.D., Norry, M.J. (eds), *Magmatism in Ocean Basins*. Geological Society, Special Publications, London **8**, 313–345.

Tatsumi, Y. & Koyaguchi, T. 1989. An absarokite from a phlogopite lherzolite source. *Contributions to Mineralogy and Petrology* **102**, 34–40.

Torabi, Gh. 1997. *Geological and Petrological Studies of the Qaleh-Khargooshi Shoshonitic Association (Sarve-Bala, west of the Yazd province, Iran)*. MSc Thesis, Geology Department, University of Isfahan, Iran [unpublished].

Wang, W. & Gasparik, T. 2001. Metasomatic clinopyroxene inclusions in diamonds from the Liaoning province, China. *Geochimica et Cosmochimica Acta* **65**, 611–620.

Wark, D.A. & Stimac, J.A. 1992. Origin of mantled (rapakivi) feldspars: experimental evidence of a dissolution- and diffusion-controlled mechanism. *Contributions to Mineralogy and Petrology* **111**, 345–361.

Watson, E.B. 1982. Basalt contamination by continental crust: some experiments and models. *Contributions to Mineralogy and Petrology* **80**, 73–87.

Wimmenauer W. 1985. *Petrography of Magmatic and Metamorphic Rocks*. Stuttgart, Germany: Enke [in German].

Yanagi, T. & Yamashita, K. 1994. Genesis of continental crust under island arc conditions. *Lithos* **33**, 209–223.